Report on the ILC Positron Source

Positron Working Group

May 23, 2018

EDMS Nr.: D00000001165115 Rev: B Ver: 3 Status: Released - for publication Dat.: 23. May 2018

Contents

EDMS Nr.: D00000001165115 Rev: B Ver: 3 Status: Released - for publication Dat.: 23. May 2018

Chapter 1

Introduction

1.1 Two Schemes of Positron Production

The ILC requires very high intensity positrons, over 10^{14} per second, hence the development of the positron source is one of the most challenging area in the ILC.

The "undulator scheme" has been adopted since the start of ILC project in 2005 as the baseline. In this scheme high-energy photons over $\sim$10 MeV are emitted from high-energy electrons over $\sim$100GeV when the latter go through short-pitch undulators. These photons are irradiated on a target and create electron-positron pairs. This method was proposed long ago but has never been adopted in real accelerators due to the obvious reason, *i.e.*, there has been no electron beam over 100GeV. Although there is no fundamental problem in the principle, the lack of experience demanded a back-up scheme, namely "electron-driven" (e-driven) scheme. This scheme has also been studied in parallel since 2005.

The advantages of the undulator scheme are:

(A) The photons are circularly polarized, hence the created positrons are logitudinally polarized, if the helical undulator is adopted.

(B) The first process in the target is the pair creation, whereas it is the bremsstrahlung in the e-driven scheme. The target can therefore be much thinner than in the latter, hence the energy deposit in the target is significantly lower. This results in the following advantages:

  - less total energy deposit on the target
  - lower radiation level in the target region
  - less demanding dynamic aperture of the damping ring

The disadvantages are:

(a) A very high energy electron beam is needed. This is not a disadvantage for the ILC because high energy electron beam is there. Nonetheless, it still causes a problem of positron production at low center-of-mass energy experiments.

(b) There is no freedom in the format of the photon beam (must be the same as that of the colliding beam).

(c) A special constraint on the orbit length, in particular the positron orbit length, is imposed.

(d) The commissioning program can be complex.

The disadvantages (b), (c), and (d) all come from the fact that the electron beam going to the interaction point is used for the positron production.

There have been several changes as the R&D progress since the initial discussion.

(B) is certainly an advantage, but the targetry technology is not simple due to the disadvantage (b) (long pulse, large pulse energy), which results in rapid rotation (100m/s) of the target and a long flat-top (∼1 ms) of the flux concentrator, etc. In the case of e-driven scheme the drive beam format can be optimized so as to relax the heat/stress load on the target. The design progress of the damping ring has brought about much larger dynamic aperture, which can accept lower quality beam. It was initially thought that more than one target were necessary in the e-driven scheme, but now a single target is thought to be enough. The advantage of lower radiation level in the target region is still an advantage of the undulator scheme. This has some impact on the CFS design, though this is not a feasibility issue but a cost issue.

Hence, by now, the main advantage of the undulator scheme is (A), *i.e.*, positron polarization.

The short-pitch undulator was thought to be the most challenging item in the undulator scheme so that its R&D studies were done in an early stage of the ILC development. The development at the Cockcroft institute was quite successful[4]. However, the rotating target in vacuum and the flux concentrator of a long pulse turned out not to be trivial. The experiments at the LLNL were not satisfactory. Therefore, we are still continuing the R&D works for the baseline and the backup schemee in parallel.

The Technical Design Report (TDR) of ILC was published in 2013. There have been significant changes in the design and the progress of the R&D studies since then. A decision on the ILC project is coming soon. It is time to summarize the works up to now and the future scope for the positron source.

1.2 Positron Working Group

The positron working group was formed under LCC-ILC in early 2017 in order

- to evaluate the technical status of the undulator and e-driven schemes for the center-of-mass energy 250GeV,
- to consider essential R&Ds in 2018-2019,
- and to compare the cost of the two schemes.

The member names are given in the appendix. The working group was demanded to submit the final report by June 2017.

Through the phone meetings every other week and face-to-face meetings in a few occasions, the technical status was summarized and presented in AWLC2017 at SLAC, and the cost comparison was presented in LCWS2017 at Strasbourg. The final report, however, was not completed by the target date.

EDMS Nr.: D00000001165115 Rev: B Ver: 3 Status: Released - for publication Dat.: 23. May 2018

1.3 Purpose of the Present Report

The major purpose of the present report is to fullfill the mission of the working group listed above. In the near future the ILC team must finally choose the approriate scheme of positron production. This report should serve as the source of basic information together with the report written by the physics team on the merit of positron polarization[2].

The TDR describes the undulator scheme in detail as the baseline choice, but it gives only a very brief description of the e-driven scheme. Thus, this report is also intended to give a systematic, consistent descrition of the e-driven schem (See Sec.3.1).

However, one and half year from the establishment of the working group was far from sufficient for the study of the whole issues on the positron production. We concentrated on the urgent issues that must be cleared before the project approval of ILC. Issues that can be studied later are mostly postponed.

The basic beam parameters of the ILC we adopted here are shown in Table 1.1.

Table 1.1: Basic Beam Parameters

Electron beam energy	125	GeV
Number of particles in the bunch	2×10^{10}	
Number of bunches per pulse	1312	
Repetition rate	5	Hz
Main linac bunch separation	554	ns
Bunch separation in damping rings	6.15	ns
Damping ring injection acceptance		
Normalized betatron amplitude $(a_x + a_y)_{\max}$	0.07	mrad
Longitudinal emittance $(\Delta E/E \times \Delta z)_{\max}$	0.75×33	$\% \times$ mm

These parameters are intended for the case $E_{CM} = 250$ GeV. When the machine is to be upgraded to higher luminosities or higher energies, the requirement of some of the parameters for the positron source must be changed. However, it should be kept in mind that the operation of the first stage will continue for many years. It should also be noted that the technically most difficult areas (for both schemes) of the prositron production, *i.e.*, the target and the first part of the capture system, are a sort of “consumable devices”. Their expected life is anyway limited, much shorter than the operation period of $E_{CM} =$ 250 GeV. They will be relaced with improved ones at the time of upgrade.

This report is a snap shot of our studies as of spring 2018.. We tried to give consistent parameters as far as we could but it is inevitable that some of the parameters contain small inconsistencies.

EDMS Nr.: D00000001165115 Rev: B Ver: 3 Status: Released - for publication Dat.: 23. May 2018

Chapter 2

Undulator Scheme

2.1 Change of the Design for Ee=125GeV

TDR described the positron production system based on the undulators, but there have been several design changes since TDR, although these changes have not yet been submitted to the Change Management procedure. They can be classified into two categories.

- Changes after the R&D studies of devices.
- Changes for concentrating the center-of-mass energy to 250GeV.

2.1.1 Hardware Changes

The former category includes the following changes:

From water cooling target to radiation cooling

TDR described water-cooled, rotating, Titanium target in vacuum. The adopted design included vacuum seal using magnetic fluid. However, its R&D studies did not go well because of the vacuum leak. This has not been proved impossible. In fact the same method is adopted for the e-driven system and in good shape in R&D. If the rotation speed (5m/s at the target rim for e-driven and 100m/s for undulator) does not make the essential difference, then the water-cooling may still be feasible for the undulator scheme. This is quite uncertain now, however. Thus, we turned to the rotating target cooled by thermal radiation. This is described in Sec.2.2.1.

From FC (Flux Concentrator) to QWT (Quarter Wave Transformer)

TDR adopted the FC as the first device for positron capture after the target. As described in Sec.2.5, however, the FC with a long flat-top (≈1ms) has a fundamental problem of field variation in time. It seems safer to replace FC with QWT, though the expected positron yield with QWT is somewhat lower than with FC.

2.1.2 Changes for the center-of-mass energy 250GeV

Length of the undulator section

A pair of undulators, each having the field length 1.75m, is stored in a cryostat. In the TDR there are 42 pairs of undulators, the total field length being 147m. This is sufficient to produce 3×10^{10} positrons per bunch (margin factor 1.5) at the electron energy over 150GeV. For the operation below the center-of-mass energy $150 \times 2 = 300$GeV TDR adopts the so-called "5+5Hz" operation, *i.e.*, 5Hz for colliding beam with $E_e = 125 GeV$ and 5Hz for positron production at $E_e \geq$150GeV.

If we concentrate on the operation at $E_{CM} = 250$GeV for many years, however, it is desirable to lengthen the undulator section for avoiding the "5+5Hz" operation. We decided to adopt the total undulator length 231m (66 pairs). The advantages are

- The maximum electron energy 125GeV rather than 150GeV
- Much lower power consumption because the pulse only to create positrons is absent
- No complication of linac operation of alternating energy. (For "5+5Hz" operation the linac accelerating gradient, hence the klystron output power, must be alternating at 5Hz.)

The only disadvantage is the increased load on the target by factor $231/147 = 1.57$.

Distance between undulator and target

In the TDR the distance between the center of the undulators and the target is chosen to be 400m. This is appropriate for $E_e \geq 150$GeV, but too long for $E_e = 125$GeV because of the larger photon spot size due to the larger opening angle ($\propto 1/\gamma$) of photons. We decided to move the undulators by about 169m downstream. According to this change the dogleg section right after the undulators for separating the photons and electrons must be shortened[3]. (See Figure 2.1.)

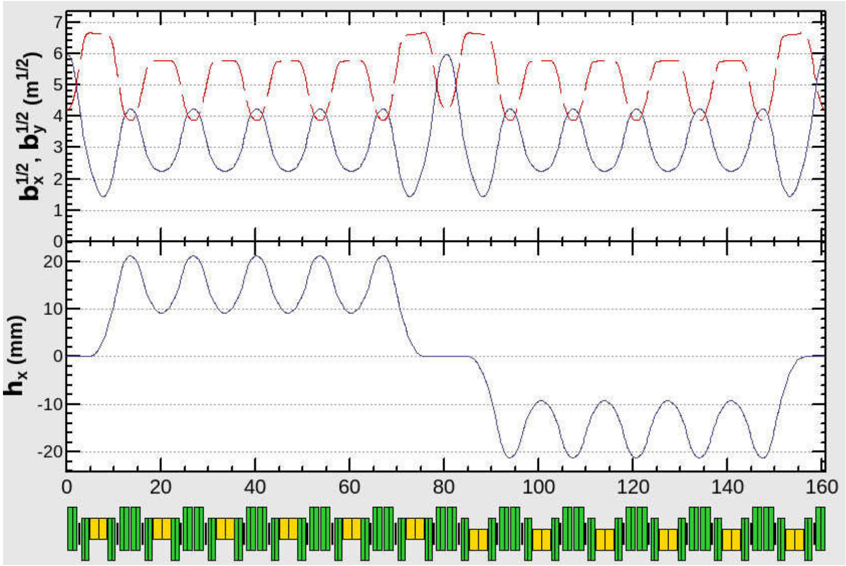

Figure 2.1: Dog-leg design for 125GeV electron beam, consisting of 12 cell (8 normal cells and 4 dispersion suppressor cells). The distance between undulator to target is shortened by 168.8 m. The horizontal offset between the electron BDS and the positron line is kept to be 1.555 m. Horizontal emittance growth for 125 GeV beam is 0.7 %. Maximum field gradients for quads are less than 60 T/m.

EDMS Nr.: D00000001165115 Rev: B Ver: 3 Status: Released - for publication Dat.: 23. May 2018

Target thickness

The TDR adopted Titanium alloy (Ti6Al4V) target with thickness 14mm. A detailed analysis revealed that the shower developed in the target create large angle secondaries which can hit the nose of the capture device when the electron energy is low. A thinner target will prevent large angle shower while producing similar number of positrons with much lower energy deposit in the target. We decided to adopt 7mm as the target thickness for $E_e = 125$ GeV. See the next subsection for the details.

2.1.3 Revised Estimation of the Positron Yield

For more details in this subsection, see [8].

Problems with Flux Concentrator

The undulator system decribed in the TDR is the one optimized for the electron beam energy 150GeV. The average photon energy from the undulators with the pitch 11.5mm and K=0.92 is 10.7 MeV. To obtain the positron yield per incident electron 1.5 the total undulator length 147m is sufficient, using the flux concentrator (FC) with the peak field 3.2 Teslas, the aperture radius 6.5mm at the nose, and the distance from the rear face of the target to the front face of FC 8 mm. The thickness of the target made of Ti6Al4V is 0.4 radiation length (14 mm).

For the electron energy 125GeV the total undulator length must be increased to 231m to reach the desired yield 1.5. The PEDD (peak energy deposit density) of the target can be reduced to a tolerable level 44 J/(g pulse). Heating of the target is acceptable with the target rotation speed 100m/s at the rim.

However, a new problem with the flux concentrator at 125GeV has been pointed out last year. The PEDD at the tip of FC turned out to be very high. The radial profile of the energy deposited in the hottest area of the FC (i.e. near the frontsurface) is shown in Figure 2.2 (right). The estimated maximum PEDD is 33.3 J/(g pulse), whereas the limit for copper is in the range 7-12 J/g.[34]. In order to relax this problem the following measures have been taken.

(a) Since the opening angle of photons is proportional to $1/\gamma$, the photon spot on the target is larger than at 150GeV. Accordingly, the distance from the undulator to the target was reduced as described in Sec.2.1. This change alone can reduce the PEDD only slightly from 33.3 to 29.3 J/(g pulse) (K=0.85).

(b) The electro-magnetic shower developed in the target has a larger angle because the average photon energy from 125GeV electron is significantly lower ($\sim$8 MeV, proportional to E_e^2). This effect can be relaxed by making the target thinner.

(c) Since the average photon energy is low, there are many photons that cannot create electron-positron pairs. They are in the peripheral part of the photon flux, and therefore, can be eliminated by a collimator just in front of the target. (Here, we chose collimation radius 2.5mm, which is much larger than the collimator for improving the positron polarization in the future, thus technically much easier. Nonetheless, a detailed study is needed.)

Figure 2.3 shows the dependence of the positron yield on the target thickness. We choose 7mm ($\approx 0.2X_0$). The above three measures relax the PEDD on the FC to 18.5 J/(g

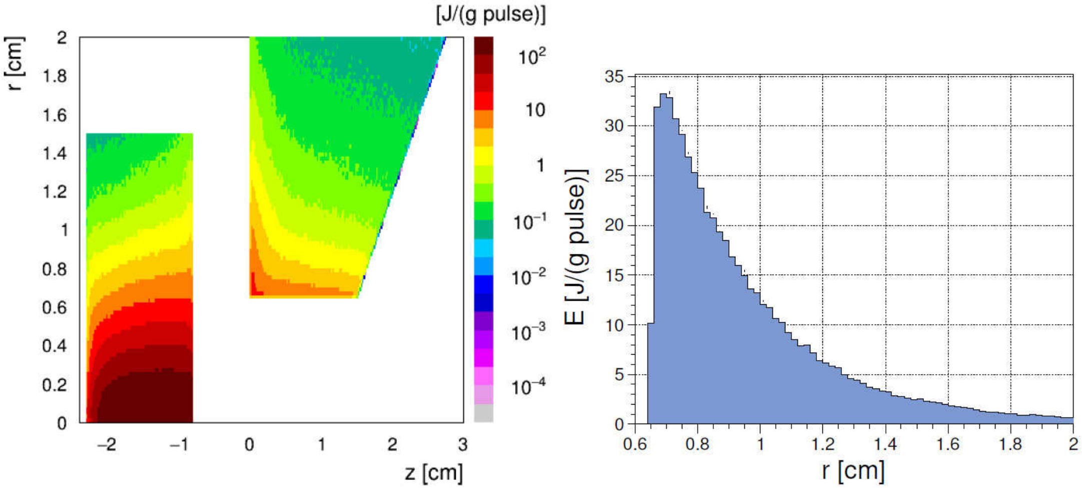

Figure 2.2: The energy deposition in the target and FC (3.2 T pulsed, aperture radius 6.5 mm) on the left. The radial profile of the deposited energy near the front surface of the FC (right). The energy deposit in the target appears very high here but this is because the target rotation is not taken into accout here.

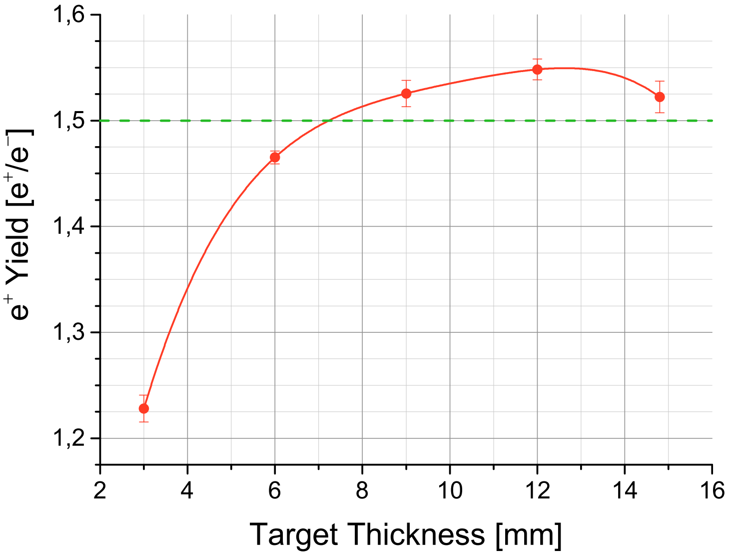

Figure 2.3: Positron yield as a function of the target thickness. Flux concentrator is used. $K = 0.85$. E_e(average)=125GeV. The yield calculation is only approximate (linear transformation from the capture section to the damping ring). The yield turned out not to be a strong function of the thickness for $>\sim$ 7mm.

pulse). Enlarging the nose aperture from 6.5mm to 8mm can further reduce the PEDD to a (marginally) tolerable level 12 J/(g pulse).

However, it is still questionable whether the nose aperture can be reduced because of the strong dependence of the required power of the FC. Moreover, a strong time-dependence of the field of the long pulse FC has been pointed out. It turned out the transverse field of FC also strongly depends on the time. (See Sec.2.5.)

The measure (b) has a byproduct (actually this is even more important), *i.e.*, the power deposit on the target is greatly reduced by making the target thinner as ashown in Figure 2.4). If the thickness is 7mm, the power deposite on the target is less than 2kW.

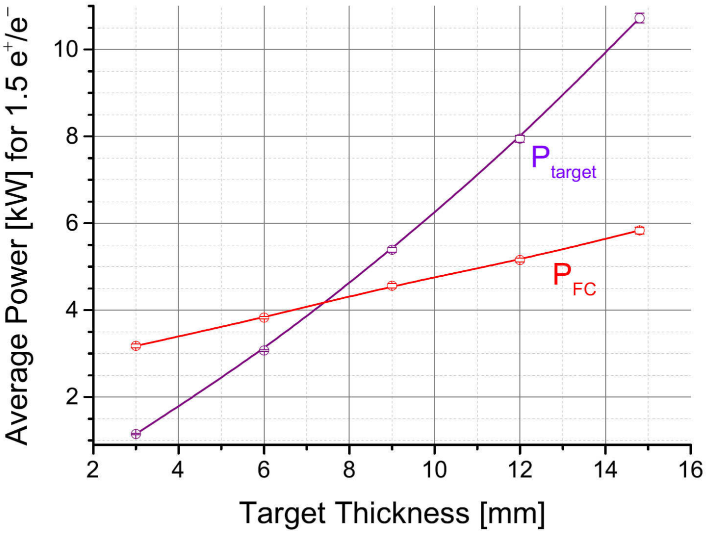

Figure 2.4: Power deposit of the target and FC as functions of the target thickness. The undulator length is adjusted for fixed yield e^+/e^-=1.5. Here, the number of bunches per pulse is 2625. The power should be halved for 1312 bunches.

Quarter Wave Transformer (QWT)

Since the FC turned out to have several difficulties, we examined the QWT (Quarter Wave Transformer) instead of FC. This possibility has been studied long ago in the early stage of ILC design, but was abondoned because the expected positron yield was significantly lower than with FC (about a factor 1.6). Now, we re-examined the possibility of QWT. We adopted the QWT designed by the ANL team with the maximum field 1.04 Tesla (See Figure 2.5). It is placed at 8mm from the rear face of the target. The radius at the nose tip is 11mm. The significantly larger aperture, 11mm compared with 6.5mm for FC, greatly reduce the PEDD at the nose to a tolerable value 7 J/(g pulse). (The upper limit of the ARMCO pure steel is 12.5 J/(g pulse).)

The improvements (a)(b)(c) are also very useful for QWT. In partucular (b) (with thickness 7mm) reduces the total energy deposit on the target by factor ≈ 3.

The distribution of the radiation damage in the QWT is very similar to the distribution of the energy deposit. The peak value of the 'displacement per atom' after 5000 hours of operation is 0.12 dpa. If 0.5dpa is considered to be the limit of the damage, then the QWT can be used for several years, longer than the desired life of the target system.

EDMS Nr.: D00000001165115 Rev: B Ver: 3 Status: Released - for publication Dat.: 23. May 2018

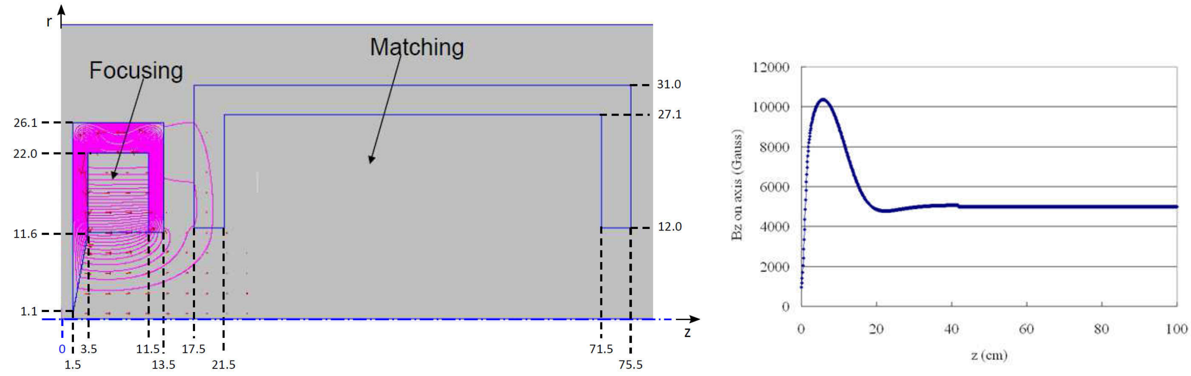

Figure 2.5: Geometry of QWT and its field on the axis. Based on the model by W. Gai and W. Liu (ANL) with dimension reporoduced by M. Fukuda. Units in cm. The field on the target is compensated for by the mirror-image pole on the left hand side. Peak field 1.04T, Solenoid 0.5T.

There are still several issues yet to be studied for QWT. For example, temperature of the nose tip and the cooling method have to be studied. The heating of the rotating target by the eddy current due to the QWT field ($O(0.05\text{T})$ on the surface) must be taken into acount. This is related to the choice of DC or pulsed. Field dragging in the space between the rear of the wheel and further along z into the QWT will occur. This effect must be evaluated.

Detailed estimation of the positron yield with QWT

An acccurate simulation of the positron yield with the above mentioned QWT has been performed using the following parameters

Undulator field length	231	m
Undulator K value	0.85	
Maximum magnetic field of QWT	1.04	T
Magnetic field at the center of target thickness	0.0	T
Distance between the rear face of target to QWT	8	mm
Minimum aperture radius of QWT	11	mm
Solenoid field	0.5	T
Aperture of the capture section	46	mm

Photon distribution as accurate as possible is used. It includes the electron energy variation from 128 to 125 GeV, betatron oscillation of electrons in the undulator section, and the masks to protect the undulators from photons, but the misalignment in the undulator section (in particular the quadrupole magnets) are not included.

The obtained yield e^+/e^- was 1.36.

TDR adopted the design yield 1.5 including the margin. The above value is a little lower than this. If everything works as calculated, 1.0 is sufficient, of course. If the above value 1.36 is judged not to be enough, the length of the undulators must be increased by ∼10%, which also means an increase of the heat load on the target by ∼10%. Another solution is to raise the K-value of the undulators slightly with the undulator length unchanged. The maximum value $K = 0.92$ of the undulator seems to give a value close

EDMS Nr.: D00000001165115 Rev: B Ver: 3 Status: Released - for publication Dat.: 23. May 2018

to 1.5, but this also means a slight increase of the target heating. Which is better should be discussed.

Undulator Field Errors

A pair of the prototype helical undulators was built at Cockcroft Institute [4] several year ago. The field intensity was sufficient but the integrated field, which must vanish, was still large. The deflection angle in one undulator exceeded the photon emission angle $1/\gamma$.

A simulation[5] was done for the electron orbit correction by using the steering magnets at every quads in the undulator section, assuming random kick of 5μrad (r. m. s.) by individual undulators, which is the larger among the two measured values. Note that the one unit of the undulator section consists of a quad, horizontal/vertical steerings followed by 6 undulators (3 pairs). The correction was done by exciting the undulators in one unit, unit by unit, and adjusted the steering magnets in this unit so that the photons correctly hit the target.

Figure 2.6 shows the photon spot size and the positron yield. Above stated steering distribution is almost sufficient to reproduce the yield without errors although the photon spot size is significantly larger than the case without errors. The spot size is better if the steering magnets are located at every 2 undulators. It can also be seen that the yield with QWT is lower than with FC but is less sensitive to the spot size (presumably due to the larger aperture).

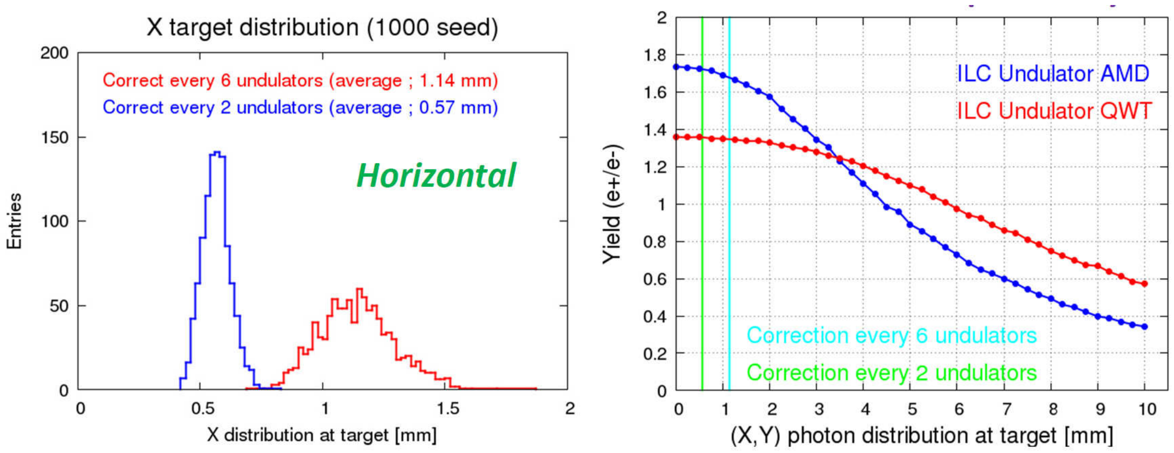

Figure 2.6: The left hand side is the horizontal photon spot size (r. m. s.) at the target under the undulator field error and correction. The distribution of 1000 random number sets is shown. The vertical spot size is similar (slightly smaller). The right hand side is the positron yield as a function of the r. m. s. spot size. The upper and the lower curves are the cases of FC (AMD) and QWT, respectively. The 2 vertical lines indicates the resulting spot size after the correction with steerings every 2 undulators (left) and 6 undulators (right).

2.2 Target for the Undulator Scheme

2.2.1 Target design progress for the undulator-based positron source

The baseline design for the ILC positron source [6] uses a long helical undulator passed by the high energy electron beam to create an intense circularly polarized photon beam. The photon beam hits a thin conversion target to produce electron-positron pairs. The target is designed as wheel of 1 m diameter and spinning with 2000 rounds per minute in vacuum. This avoids overheating of the target material which is currently specified as Ti6Al4V. Since the average energy deposition in the target is only few kW, cooling by thermal radiation is a promising option which is currently studied. The status is presented here with focus on the $E_{\mathrm{cm}} = 250\,\mathrm{GeV}$ option.

The photon yield and energy depend strongly on the electron energy. The photon yield decreases with the electron energy and has to be compensated by a longer undulator. The narrow photon beam causes a high peak energy deposition density (PEDD) on the spinning target. Studies [9] showed that for $E_{\mathrm{cm}} = 250\,\mathrm{GeV}$ a reduced target thickness does not reduce the positron yield but decreases substantially the energy deposition in the target. Hence, for the 250 GeV option the target thickness is 7 mm. Table 2.1 summarizes the parameters to achieve a positron yield of $Y = 1.5\,\mathrm{e}^+/\mathrm{e}^-$ [7]; for completeness also the parameters for higher centre-of-mass energies are listed. For the 250 GeV option the energy deposition in the inner part of the flux concentrator front side is too high. To resolve this problem, the drift space between undulator and target could be reduced. Alternatively, a quarter wave transformer could be used. Further details can be found in reference [8] (Also, see Sec.2.1). Definitely, a distance of 401 m between middle of the undulator and target represents the case with highest load. Thus, this option is studied and the results are presented here.

2.2.2 Cooling by thermal radiation

Following the Stefan-Boltzmann law,

$$P = \sigma_0 \varepsilon_{\mathrm{eff}} A (T^4 - T_0^4)\,, \tag{2.1}$$

with $\sigma_0 = 5.67 \times 10^{-12}\,\mathrm{W/(cm^2\,K^4)}$, the effective emissivity $\varepsilon_{\mathrm{eff}}$ and the radiating surface A. One finds that $A = 0.36\,\mathrm{m}^2$ is required to remove 2 kW if the average temperature is $T_{\mathrm{ave}} = 400°\mathrm{C}$ and $\varepsilon_{\mathrm{eff}} = 0.5$. For comparison: the area of a ring with outer diameter $r_o = 51\,\mathrm{cm}$ and inner diameter $r_i = 45\,\mathrm{cm}$ is $0.36\,\mathrm{m}^2$ taking into account front and back side. With other words: The wheel spinning in vacuum can radiate the heat to a stationary cooler opposite to the wheel surface. The cooler temperature can be easily kept at room temperature by water cooling. But a crucial item for the design is the heat distribution from the volume heated by the photon beam path to a larger surface area. Due to the low thermal conductivity of Ti6Al4V, $\lambda = 0.068\,\mathrm{W/(cm\,K)}$ at room temperatures and $0.126\,\mathrm{W/(cm\,K)}$ at 540°C, the time between beam impacts at the same target position is not sufficient to distribute the heat almost uniformly over a larger volume. Instead, the heat is accumulated in the rim and the highest temperatures are located in a relatively small region around the beam path. A substantial part of the deposited power is radiated from that outer area.

EDMS Nr.: D00000001165115 Rev: B Ver: 3 Status: Released - for publication Dat.: 23. May 2018

electron beam energy	GeV	126.5	125	150	175	250
undulator active length	m	231		147		
undulator K		0.85		0.8	0.66	0.45
photon yield per m undulator	$\gamma/(e^- m)$	1.70		1.52	1.07	0.52
photon yield	γ/e^-	392.7		223.9	157.3	76.1
photon energy (1st harmonic)	MeV	7.7	7.5	11.3	17.6	42.9
average photon energy	MeV	7.5	7.3	10.4	13.7	26.8
average photon beam power	kW	62.6	60.2	48.8	45.2	42.9
photon bunch energy	J	9.6	9.2	7.4	6.9	6.5
electron energy loss in undulator	GeV	3.0	2.9	2.3	2.2.	2.0
Ti6Al4V target thickness	mm	7	14.8	14.8		
energy deposition per photon in target	MeV	0.23	0.7	0.8	1.0	1.4
relative energy deposition	%	3.1	9.0	8.0	7.3	5.3
average power deposited in target	kW	1.94	5.4	3.9	3.3	2.3
energy deposition per bunch	J	0.3	0.83	0.60	0.50	0.35
space from middle of undulator to target	m	401	570	500		
photon beam spot size on target (σ)	mm	1.2	1.72	1.21	0.89	0.50
PEDD in target per bunch	J/g	0.65	0.40	0.49	0.66	1.19
PEDD in target per pulse (100 m/s)	J/g	61.0	43.7	41.0	42.4	45.8
polarization of captured positrons at DR	%	29.5	30.7	29.4	30.8	24.9

Table 2.1: Summary of the source performance parameters for different energies and 1312 bunches per pulse. The repetition rate is 5Hz. The numbers are shown for a decelerating capture field. A flux concentrator is assumed for the studies. See also references [6, 7, 9].

Several ideas to design a radiation cooled positron target are under consideration. The 2 kW energy deposition expected for the $E_{\mathrm{cm}} = 250\,\mathrm{GeV}$ option suggests to use a full disc wheel consisting of the target material with the required thickness. This case is considered here.

2.2.3 Load limits in Ti6Al4V

So far, the boundary conditions for design considerations are based on data sheets from vendors of Ti6Al4V, and studies [13] that showed that for irradiated Ti6Al4V the material parameters change. It is not so easy to define the maximum allowed load for the irradiated target, experimental tests are necessary. We performed tests at the Microtron in Mainz (MAMI) which imitated the ILC cyclic and long-term load [22]. The irradiation of target samples (size 1.5 cm×4.2 cm) demonstrated that Ti6Al4V stands the very high load with about 6×10^6 load cycles (corresponding to roughly 2 years ILC operation). Based on this encouraging result FEM studies are performed to evaluate the temperature and stress distribution in the target wheel. As rough benchmark for these studies a total load of 400–500 MPa is assumed as ultimate upper limit.
The damage of the target material due to irradition is 0.04 dpa/year, see [23].

EDMS Nr.: D00000001165115 Rev: B Ver: 3 Status: Released - for publication Dat.: 23. May 2018

2.2.4 Stationary temperature and stress distribution

The temperature distribution in the target wheel determines the stress development in the target. Due to the low thermal conductivity the temperature gradient along the radius is large. At elevated temperatures the material will expand; the highest thermomechanical stress is expected in the rim region of the target disc.

Simulations with ANSYS [19] were performed to study the temperature distribution and the corresponding thermal stress. The temperature dependence of the material parameters (thermal conductivity, heat cappacity) was taken into account (see also reference [11]).

For the disc target design two options are under study:

- The target is a simple disc with a hole for mounting.
- The target disc has expansion slots to reduce the thermal stress in the rim region.

For each of these options the following target parameters are varied:

1. length of the expansion slots
2. emissivities of target surface and cooler
3. distance between cooler and target surface
4. distance between radius of the beam path on the disc and radius of the wheel

The use of expansion slots was already discussed in reference [11]. With expansion slots the stress in the target rim is not a problem. However, the wheel frequency and beam pulse must be synchronised very carefully which needs additional equipment. New simulations take into account all parameters temperature dependent, *i.e.* also the modulus of elasticity. It figured out that E drops with rising temperature (see Figure 2.7) so that the stress values in the rim given in Table 3 of reference [11] decrease.

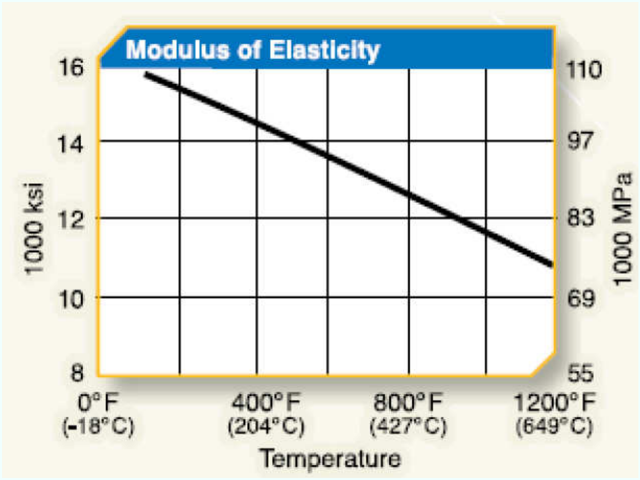

Figure 2.7: The modulus of elasticity dependent for Ti6Al4V (Grade 5) depending on the temperature taken from reference [12] (www.atimetals.com).

The radial temperature distribution in the disc is shown in Figure 2.8. It summarizes representative radial temperature profiles depending on the emissivities of the target and

EDMS Nr.: D00000001165115 Rev: B Ver: 3 Status: Released - for publication Dat.: 23. May 2018

cooler material for a solid disc of 51 cm and 52.5 cm radius; the beam hits the target at a radius of 50 cm. Larger wheel radii increase slightly the radiative area in the hot rim region and decrease the maximum temperature.
We also tested the influence of the distance between target surface and cooler which affects the radiating geometry in the hot rim region. It was found that this influence on the temperature is almost negligible.
The emissivity of the Ti6Al4V target sample used in the irradiation experiment at MAMI was measured to $\varepsilon \approx 0.5$. So it is expected that at least target and cooler surfaces with emissivities of 0.5 are feasable. This would result in an effective emissivity of ≈ 0.33 for the thermal radiation. As shown in Figure 2.8, in such case the maximum average temperature is roughly 460°C, almost 100 K lower than for the case with $\varepsilon_{\text{eff}} \approx 0.19$ considered in reference [11]. Table 2.2 summarizes the maximum average temperatures

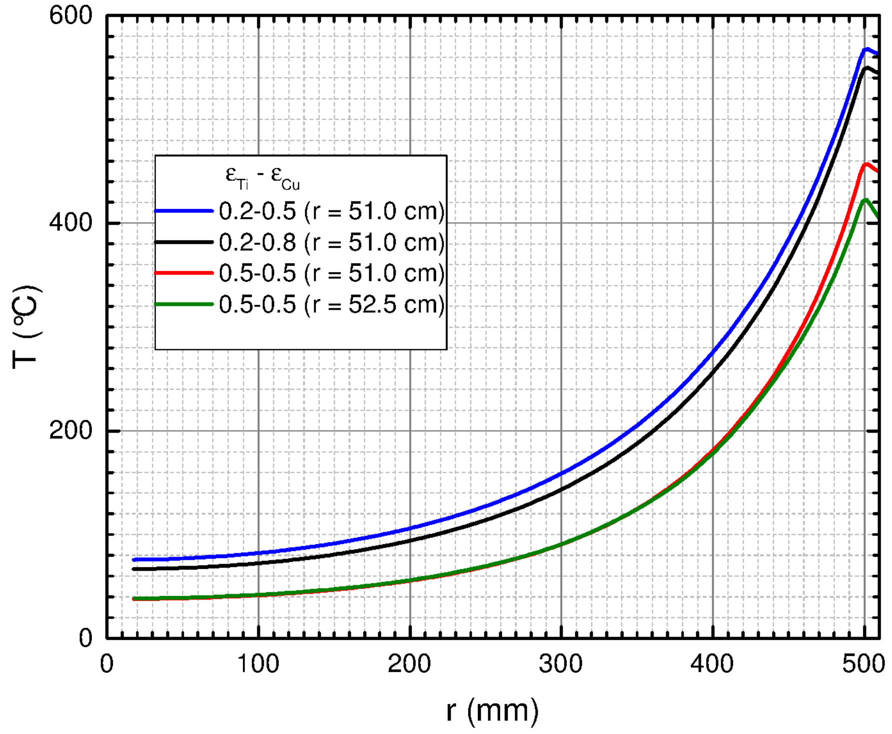

Figure 2.8: Radial average temperature distribution in the target wheel without radial expansion slots for various emissivities of target and cooler (copper). The beam hits the target at a radius of 50 cm. The outer wheel radius is 51 cm and also 52.5 cm.

for several assumed emissivities and wheel radii.

The distribution of the von Mises stress is shown in figure 2.10 of section 2.2.6.

2.2.5 Cyclic load

In addition to the high average temperatures in the rim region the photon beam creates cyclic load in the ILC positron target which happens every 6-8 seconds at the same position depending on the wheel revolution frequency. As discussed in reference [11], the

$\varepsilon_{\mathrm{Ti}}$	$\varepsilon_{\mathrm{Cu}}$	$\varepsilon_{\mathrm{eff}}$	r_{w} [cm]	$T_{\mathrm{max}}^{\mathrm{ave}}$ [°C]
0.5	0.5	0.33	51	456
0.5	0.5	0.33	52.5	421
0.2	0.8	0.19	51	550
0.2	0.8	0.19	52	523
0.2	0.8	0.19	53	502
0.2	0.5	0.17	51	567

Table 2.2: Maximum average temperatures in the positron target disc for verious emissivities of target and cooler surfaces, $\varepsilon_{\mathrm{Ti}}$ and $\varepsilon_{\mathrm{Cu}}$, and different wheel radii, r_{w}. The beam hits the target at $r = 50\,\mathrm{cm}$. $\varepsilon_{\mathrm{eff}}$ is the approximate effective emissivity for target plus cooler.

photon beam causes an instantaneous temperature rise of about 80 K (nominal luminosity, see Table 2.1). Hence, also for low emissivities the resulting peak temperature occur only locally for short time and does not exceed 600–650°C. The cyclic temperature in the target rim caused by the beam impact is shown in figure 2.9 for an effective emissivity of $\varepsilon_{\mathrm{eff}} = 0.33$ ($\varepsilon_{\mathrm{Ti}} = \varepsilon_{\mathrm{Cu}} = 0.5$). The cyclic load creates peak temperatures up to 519°C; the maximum average temperature is 460°C.

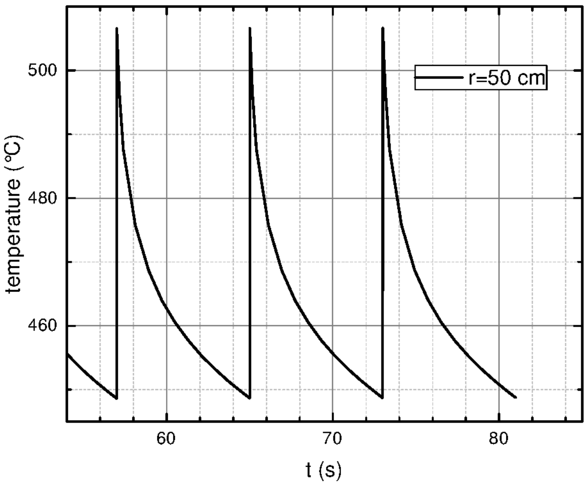

Figure 2.9: Temperature evolution in the target along the beam path with photon beam pulses. The effective emissivity is $\varepsilon_{\mathrm{eff}} = 0.33$.

It was a very important result from the MAMI experiment to see that no serious damage was obtained even at temperatures up to the phase transition point. However, it did not take into account any load from a moving target. To estimate the influence of cyclic stress at higher temperatures one must take into account that $\sigma(T) \propto E(T)$ (E is the modulus of elasticity). Using the temperature-dependent values shown in figure 2.7, the maximum load created by one pulse in a small target region is below 150 MPa, substantially lower than assumed in reference [11].

EDMS Nr.: D00000001165115 Rev: B Ver: 3 Status: Released - for publication Dat.: 23. May 2018

2.2.6 Stress due to wheel rotation

The target rotation with 2000 rpm ($\omega \approx 200$ Hz increases the stress in the wheel in radial (σ_r) and tangential (σ_H) direction.This dynamic stress at the radius r is given by [25]

$$\sigma_\mathrm{H} = \frac{3+\nu}{8}\rho\omega^2\left(1-\frac{r^2}{r_o^2}\right)\left(1-\frac{r_i^2}{r^2}\right) \quad (2.2)$$

$$\sigma_\mathrm{r} = \frac{3+\nu}{8}\rho\omega^2\left(1+\frac{r_i^2}{r_o^2}+\frac{r_i^2}{r^2}-\frac{1+3\nu}{3+\nu}\frac{r^2}{r_o^2}\right) \quad (2.3)$$

$$(2.4)$$

with the inner and outer radius r_i and r_o, the density ρ and Poisson's ratio ν. First of all it is important to note that the target rotation increases the stress in the hot target region only little: for a wheel with $r_o = 52$ cm the radial stress at the beam path radius ($r = 50$ cm) is 1.4 MPa, the hoop stress along the beam path is 8.7 MPa. The maximum hoop stress occurs at the inner wheel radius and is about 40 MPa. The maximum radial stress is located at $r = \sqrt{r_o r_i}$, *i.e.* at $r \approx$ 10...16 cm depending on $r_i =$ 2...5 cm. In this region the temperature is about 100°C. Due to the simple wheel geometry without expansion slots these results agree well with that of ANSYS simulations taking into account the wheel rotation and the temperature dependent material parameters. The results of the ANSYS simulations for the stress distribution are shown in Figure 2.10 for three cases: (i) no wheel rotation, all parameters including the thermal expansion coefficient α and the modulus of elasticity E are taken temperature dependent; (ii) the wheel rotates with 2000rpm, all parameters are taken temperature dependent except α and E which are kept at room temperature; and (iii) the wheel rotates with 2000rpm, all parameters including α and E are temperature dependent in the simulation. In total, the peak stress due to average thermal load plus cyclic peak by beam impact is 300 MPa even if the target is a full disc without expansion slots. The stress in the wheel is compressive.

For comparison, the von Mises and also the minimal principal stress for a target wheel with expansion slots of 20 cm and 6 cm length is shown in figure 2.11.

2.2.7 Target wheel and OMD

The target wheel will be installed near to a pulsed flux concentrator (FC). Alternatively, a quarter wave transformer (QWT) can be used to capture and focus the positrons. Depending on the magnetic field that the OMD creates on target, eddy currents could increase the target temperature and could slightly drag the wheel rotation. First calculations of eddy currents as well as tests with a Ti6Al4V wheel spinning in a magnetic field have shown that eddy currents are not a serious problem for the target operation [26, 27].

The distance between target and flux concentrator or QWT must be as small as possible to achieve a high positron yield. Both, FC and QWT occupy a large area in front of the spinning target since the radii of these devices are about $25-30$ cm. When passing the area of these matching devices the hot target surface cannot radiate to the cooler surfaces. The results presented above do not take into to account the somewhat lower cooling efficiency at the level of QWT or FC. Either FC or QWT can be cooled excellently or the target temperatures are slightly higher. The heat load in the OMD coming from the radiating target has to be taken into account for its final design. If one assumes that the radiating target surface is reduced by 25% (corresponding to no cooling

EDMS Nr.: D00000001165115 Rev: B Ver: 3 Status: Released - for publication Dat.: 23. May 2018

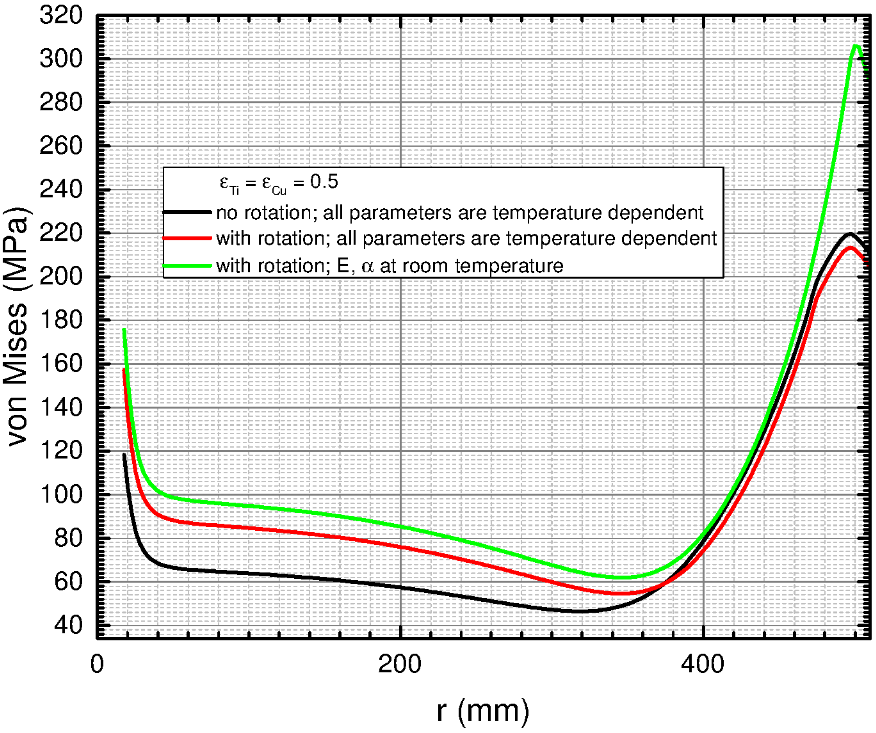

Figure 2.10: Radial distribution of average von Mises stress in the full disc target wheel without radial expansion slots. Black: no wheel rotation, all parameters are taken temperature dependent. Red: wheel rotates with 2000rpm, all parameters are taken temperature dependent. Green: wheel rotates with 2000rpm, E and α are taken at room temperature for the simulation. The beam hits the target at a radius of 50 cm.

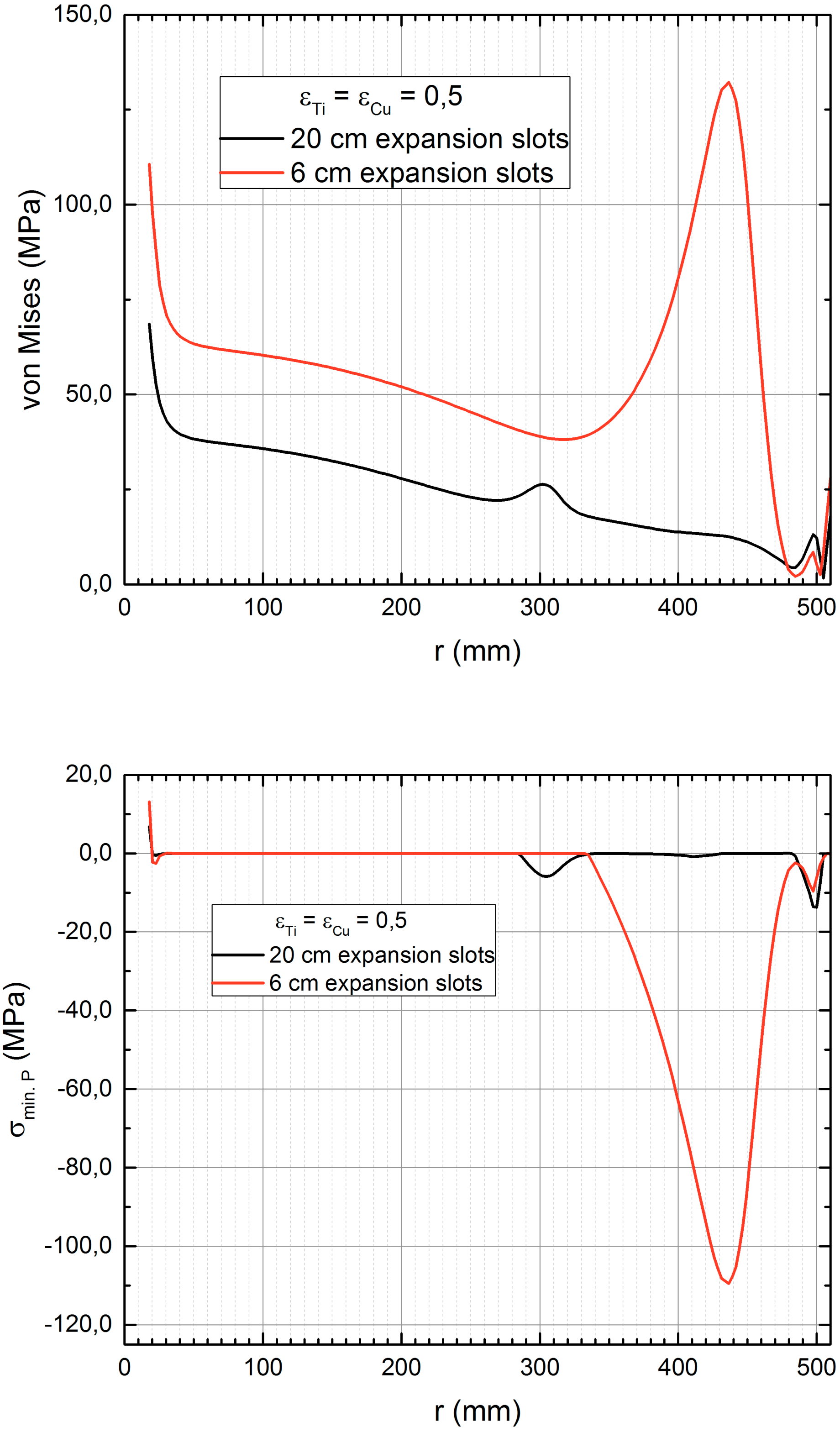

Figure 2.11: Radial distribution of average stress in the rotating target wheel with radial expansion slots of 6 cm (red) and 20 cm (black) length. Upper plot: von Mises stress; lower plot: minimal principal stress. All parameters except ε are taken temperature dependent. The beam hits the target at a radius of 50 cm; the wheel radius is 51 cm.

EDMS Nr.: D00000001165115 Rev: B Ver: 3 Status: Released - for publication Dat.: 23. May 2018

on target front and exit side in the region covered by a QWT), the maximum average temperature increases from 460oC to about 510oC (option with $\varepsilon_{\mathrm{Ti}} = \varepsilon_{\mathrm{Cu}} = 0.5$).

2.2.8 Driving mechanism and bearing

Magnetic bearings, developed for fly wheels for energy storage, for vacuum pumps and for Fermi Choppers have been developed, and are available on the market (SKF, Kernforschungszentrum Juelich), possibly to be adapted to the operating conditions of the rotating Titanium wheel for positron production. These are based on permanent magnet technology. Breidenbach *et al.* [17] have studied a bearing, based on electro-magnetic coils. Both solutions seem to be feasible. However, both of them require good radiation resistance and stability, and must be shielded. Further R&D has therefore to be envisaged.

The heating of the target yields a non-uniform temperature distribution and stress within a wheel. At a first glance [20], the corresponding deformation due to expansion does not yield imbalances of the spinning wheel. So far, the dynamic effects have not yet considered in detail. Comprehensive simulations are planned to study them in order to prepare a reliable wheel design.

2.2.9 Safety issues

The energy stored in the wheel is

$$E_{\mathrm{wheel}} = 0.5 J \omega^2 \,, \tag{2.5}$$

where J is the moment of inertia. Assuming a full disk of 52 cm radius and 2000rpm, about 72 kJ are stored in the wheel considered here for the $E_{\mathrm{cm}} = 250\,\mathrm{GeV}$ option. Appropriate housing is required. Due to the short distance to the target a protection of the OMD against mechanical crash of the target seems impossible.

2.2.10 Summary - Undulator target

The simulation and tests for the ILC250 showed that maximum temperature and stress in the target wheel are large but not too large. Even a simple wheel designed as disc without expansion lots could be feasible.

- The energy deposition in the target is about 2 kW.
- The maximum average temperature depends on the wheel design, in particular on the emissivities of the target and the surface available for radiative cooling. The latter depends also on the distance between the wheel radius and the radius of beam impact.
  Emissivities of 0.5 should be possible by appropriate surface treatment.
- The peak temperature due to cyclic beam impact is roughly 45 K higher than $T_{\mathrm{max}}^{\mathrm{ave}}$ for the example considered here (see Figure 2.9), *i.e.* the peak temperature in the target is 510°C.

EDMS Nr.: D00000001165115 Rev: B Ver: 3 Status: Released - for publication Dat.: 23. May 2018

- The highest static stress is located in the rim region due to thermal expansion. With temperature dependent material parameters one finds the maximum stress values in the beam impact region of $\sigma_{\rm vM} \approx 180\,\rm MPa$.
- The target rotation increases slightly the maximum stress values: one finds for $\varepsilon_{\rm eff} = 0.33$) maximum average stress values of $\sigma_{\rm vM}^{\rm ave,max} \approx 220\,\rm MPa$. Including the beam impact, momentary peak values below 300 MPa are expected.
- The average stress in the rim can be substantially reduced by slots which allow expansion of the hot target areas. These slots should range to the cold wheel region, *i.e.* they should be longer than 10 cm.
- Expansion slots require the synchronisation of rotation frequency with the beam impact to keep a constant luminosity during the bunch train.

Ti6Al4V is the working horse among the Titanium alloys and designed for operation temperatures below the 500°C. Meanwhile high-strength, high-temperature Ti alloys have been developed which stand higher continuous load than Ti6Al4V. An example is Ti SF-61 which is a very promising alternative as suggested in reference [17]. It is designed for continuous operation at temperatures up to 630°C and has a high endurance limit, creep resistance and fatigue limit up to 820°C [24].

2.3 Key Issues on the Target for Undulator Scheme

2.3.1 Introduction

The initial proposal for the design of the Undulator driven positron target consisted of a fast rotating Titanium wheel. To remove the power, deposited by the beam in this wheel, water cooling was envisaged. However, in view of the major technical challenges, involving Ferrofluid vacuum seals running at 33 Hz, and after inconclusive prototype tests, the need for an alternative solution arose.

Thus, during the POSIPOL 2013 workshop at Argonne-France [29], a solution was proposed to evacuate the beam power of about 4 kW from the rotating wheel by thermal radiation into a stationary water cooled heat sink. The great advantage of this solution is that no rotating vacuum seals are required. However, vacuum compatible rotating bearings, and in particular magnetic bearings, as well as sufficiently large radiating surfaces with adequate emissivity will be necessary. This will lead to considerable weight of the wheel with its diameter of one meter, spinning at 33 Hz. These studies continued and the results were regularly updated in the following POSIPOL workshops. Most recent results were presented at the ILCW in 2017 [30].

Following the recent decision to reduce the beam power, the target thickness could be reduced from 14 mm to 7 mm (see Sec.2.1.2), which leads to a power dissipation in the wheel of only 2 kW. Following the line developed in [30], in this note a technical solution is studied in which tolerable average temperatures are achieved while minimizing the weight of the wheel.

2.3.2 Computational Approach

As in initial studies[30], made with ANSYS, the average power is deposited around the outer rim of the wheel and lead by heat conduction radially towards the inner part of

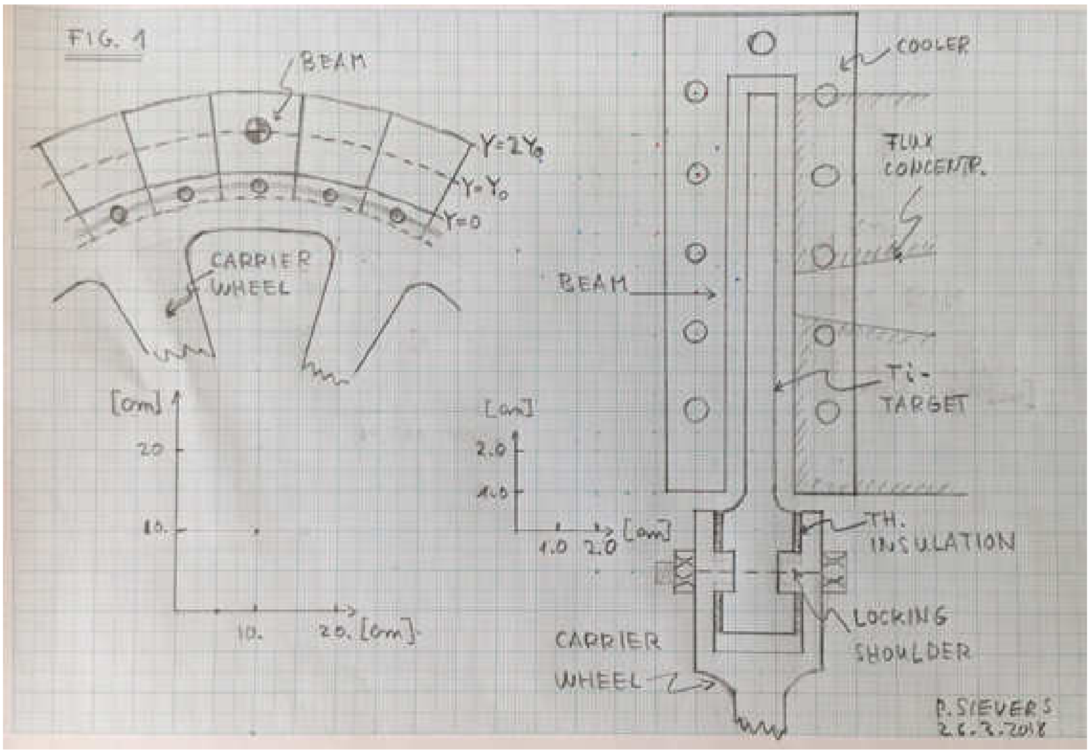

Figure 2.12: A front view and a cut through the cross section of the wheel (see the different scales). Ti-target sectors are mounted onto the carrier wheel. The water cooled stationary cooler is arranged around the rotating wheel, except for the region where the flux concentrator is placed. Details of the fixation of the target sectors to the carrier wheel are explained in the text.

the rotating wheel, from where the heat is radiated from both its side surfaces into a stationary water cooled cooler.

The issue is now to work out the radial equilibrium temperature distribution, allowing for the complete evacuation of the deposited heat by radiation.

The highest temperatures are reached at the rim and this area is thus most effective for the removal of heat by thermal radiation. Towards the inner part of the wheel, the temperature decreases and this part of the wheel contributes only little to thermal radiation.

Here a wheel is now considered where the active part of the wheel consists only of a Ti-ring of a certain height. The beam hits the line along the centre of this ring, so that now the heat can propagate into the inner as well as into the outer part of the ring. This allows to minimize the temperatures, the weight of the wheel and to improve certain engineering aspects as explained below. The layout is sketched in Figure 2.12. In this solution, the target ring is cut up into sectors, each with a width of about 10 cm and a total height of also about 10 cm. Each of those sectors is mounted onto a full carrier wheel (See Figure 2.12), leading to a structure of the whole wheel with an outside diameter of 110 cm.

To investigate the radial temperature profile across the rim, in a first approach, it can be developed in a Taylor series along the radial coordinate Y around the inside boundary of this rim at $Y = 0$, and this for small heights $2Y_0$ as compared to the radius of the wheel:

$$T(Y) = T_1(1 + aY + bY^2/Y_0 + \cdots). \tag{2.6}$$

Thus, for simplicity we can ignore the change of the surface with the radius and assume a constant, radially independent surface. Moreover, since the radial temperature distribution is symmetric about the line of impact at $Y = Y_0$, it is sufficient to consider only the region between $Y = 0$ and $Y = Y_0$, where however now only half of the total power is injected. The heat is deposited as a constant line source in time along the middle of the rim at $Y = Y_0$. Therefore the heat will propagate radially from the centreline Y_0 towards the inside up to the inner boundary at $Y = 0$, as well as of course towards to the outer boundary at $2Y_0$ of this rim.

Since we envisage for Y_0 about 5 cm (see Figure 2.12), which is small compared to the radius of the wheel of about 50 cm, the effective thermal conductance does not depend strongly on the radial position Y, and we can limit the Taylor series to the third term in Y^2.

To continue along this line, we have to find the unknown coefficients a and b as well as the temperature T_1 at the inner boundary in the Taylor series. Without presenting here the rather lengthy procedure[31] these constants can be derived from the two boundary conditions at $Y = 0$ and $Y = Y_0$ and the condition that in the equilibrium, all the input heat must finally be radiated through both sides of the Ti-rim. This leads to an equation in terms of T of up to its fourth power, which has to be solved numerically. It contains all the relevant parameters:

Input power 1 kW, half of the total power, is deposited continuously as a constant line source along the centre line along $Y = Y_0$ and to be evacuated via the inner part of the Ti-ring. This does not yet take into account that the heat input is pulsed every 6-7 s into one sector, where the pulsing is felt only over a radial width of about 5 mm. This will reduce the average temperature along this line (see later).

All other input parameters are kept constant:

- Heat input of 1 kW along a radius of 50 cm.
- Temperature of the cooler at room temperature of 300 K.
- Effective emissivity 0.2 .
- Thermal conductivity of Ti: 0.07 W/cm K.
- Target thickness 0.7 cm.

As e.g. the thermal conductivity in Ti can increase by up to a factor of two at elevated temperatures, conservative results will be achieved with some safety margin, when constant material parameters at room temperature are applied.

2.3.3 Results

Using the above input parameters, the temperature profiles along Y for total rim heights $2Y_0$ of 6 cm, 10 cm and 15 cm are displayed in Figure 2.13. As expected, the peak temperatures at $Y = Y_0$ of 550-600 ^{o}C depend only little on Y_0, while the temperatures T_1 at the boundaries are decreasing and become somehow uncritical below 300 ^{o}C , at least for $2Y_0$ of 10 cm and above.

EDMS Nr.: D00000001165115 Rev: B Ver: 3 Status: Released - for publication Dat.: 23. May 2018

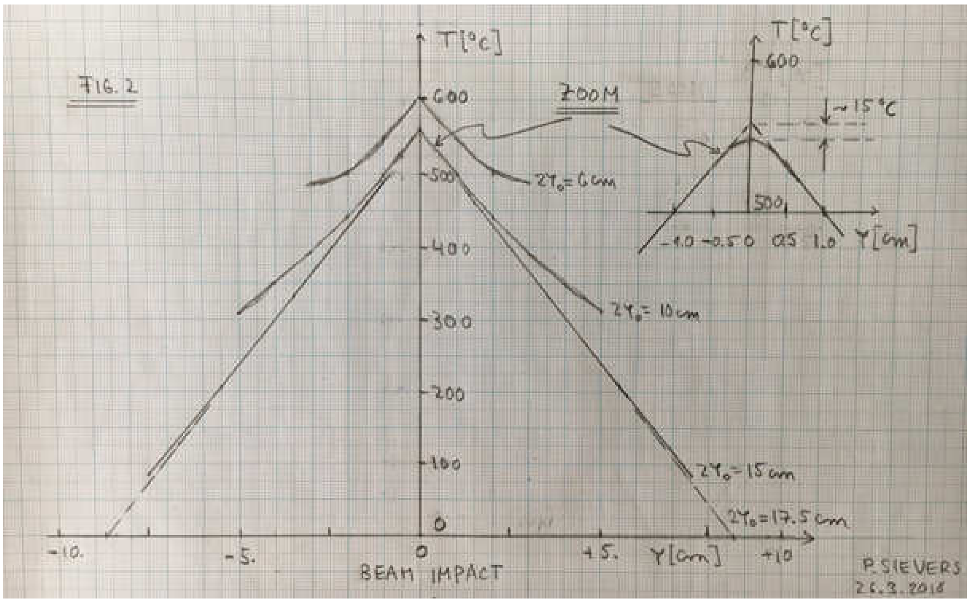

Figure 2.13: The radial temperature profile around the point of beam impact for different total heights $2Y_0$ of the target sectors, including a zoom at the centre line. The temperature of the cooler is set to zero at 300 K. The envisaged geometry with $2Y_0$=10 cm is considered as the most realistic reference case.

It is worth mentioning, that within the approximations applied here, the maximum useful height of the rim is about 18 cm, beyond which the evacuation of heat by radiation along this additional surface becomes negligible.

As mentioned above, using a continuous line source as a power input along $Y = Y_0$ leads to maximum average temperatures at this location. Since the pulsed beam hits the same part of the rim every 6-7 seconds, with a PEDD of 61 J/g and 43.7 J/g [30], the temperature per pulse will rise at this location by 105 K and 80 K respectively. But due to thermal diffusion during the down time of the beam, the heat will be spread over a total width of about 10 mm, before the next pulse arrives. As illustrated by the zoom in Figure 2.13, a reduction of the average temperature at $Y = Y_0$ at about 560 ^{o}C , by about 15 K can thus be expected. Evidently, just after a beam pulse, the temperature rise per pulse of about 80-100 ^{o}C will have to be added to the average peak temperature.

In further studies we concentrate on the most relevant case, the "Reference Case", with $2Y_0$ of 10 cm, which seems to be a good compromise. It is of importance to check how robust such a geometry is with respect to variations of the input power, the effective emissivity between Ti and Cu and the thermal conductivity of Ti. The results are shown in Figure 2.14.

As can be seen, with the envisaged geometry, the maximum power should not exceed 3 kW, giving rise to time average peak temperatures of 700 ^{o}C . Above those temperatures, the mechanical strength of Ti will be lost.

As displayed also in Figure 2.14, changes in emissivity and thermal conductivity will influence the peak temperatures. Variations of the emissivity between 0.1 and 0.3 as well as an increase of thermal conductivity from 0.07 to 0.14 W/cm K, as expected at higher temperatures, have been considered. The variations of the peak temperatures are normalized to those of the reference case. Although the relative temperatures decrease only by 10%, some 50 ^{o}C , the search for materials with higher emissivity and thermal conductivity should be pursued.

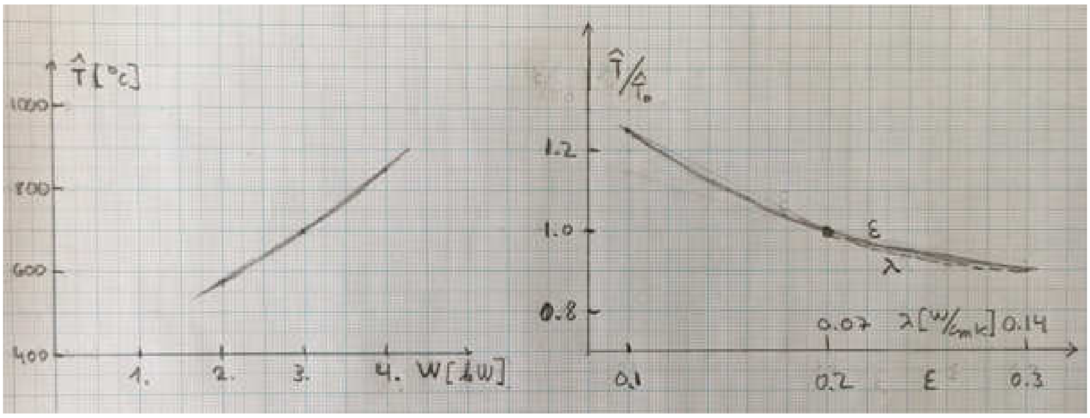

Figure 2.14: Peak temperatures in the target vrs. average input power (left), showing the distinct increase of the peak temperature with higher input powers. In the right picture, the variation of the peak temperatures, relative to the reference case (ε=0.2, λ=0.07), are shown vrs. the thermal conductivity of Ti as well as the effective emissivity of the Ti-Cu-Cooler unit. By increasing these parameters, a decrease of the peak temperature by about 10 % can be expected.

In this context, one may also consider to increase the thickness of the Ti-rim, which is outside the actual active target region, say beyond 1 cm from the centre line, from a thickness of 7 mm to 15 mm. This will increase the effective thermal conductivity of the thicker Ti-part by a factor of two. The influence of all these effects can reliably be validated by laboratory test, as described in the next chapter.

2.3.4 Thermal Tests of a Sub-Sector of the Wheel in a Laboratory Mock up

As presented at the LCWS in 2017 at Strasbourg-France[32], and later in a special dedicated meeting in 2017 at Itako-Japan[33], the evacuation of heat by thermal radiation can quite simply be validated in a lab-mock, as shown in Figure 2.15. It requires only a small, of course non rotating sector of the wheel of about 10 to 15 cm width, to be installed in a tank of rough vacuum, and to be heated by a standard electrical heating cartridge of some 100 W. Following the manufacturer's instructions, adequate thermal contact between the cartridge and the surrounding Ti-body can readily be achieved. If required, more robust thermal contacts can be devised.

This whole Ti-unit is then surrounded by a water cooled cooler. The principal layout, shown in Figure 2.15, is an update of previously presented layouts. It has to be ensured that 100 % of the electrical power is guided towards the target radiators with only small parasitic losses elsewhere. To prevent such heat leaks, like around the immediate location of the electrical heater, radiation can be suppressed there by an envelope of super insulation with several layers of Al-foils.

All the required auxiliary supplies, like electrical power, cooling water and thermocouples will be fed into the vacuum tank through its top cover flange. The size of the vacuum tank and the top flange should be generously dimensioned to allow for tests of various geometries and technical optimisations.

EDMS Nr.: D00000001165115 Rev: B Ver: 3 Status: Released - for publication Dat.: 23. May 2018

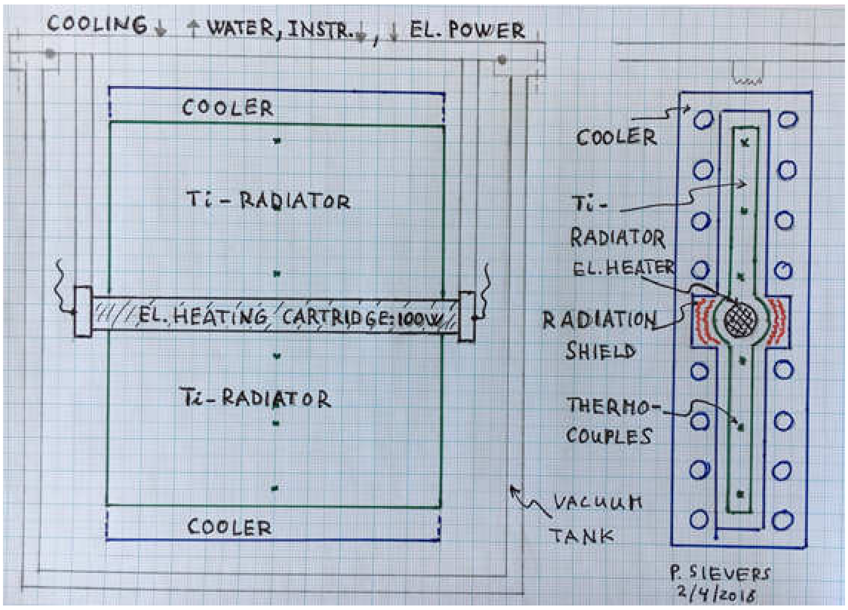

Figure 2.15: Front view and a cut through the laboratory test set up of a stationary sector of the target to validate the cooling via thermal radiation. Heat input by an electrical heater and cooling by radiation from the Ti-radiators into the coolers. All required supplies are fed in through the top flange of the vacuum vessel.

This test will produce reliable results under realistic conditions, involving all the possibly temperature dependent parameters, like thermal conductivity, emissivity and others.

2.3.5 Thermal Stresses and Centrifugal Forces

As it will not be easy to include in the above described laboratory tests also thermal stresses and fatigue effects, those will finally have to be validated separately in dedicated material test.

As sketched in Figure 2.12, the target rim is not made of one single ring, but of sectors of about 10 cm width. These are mounted onto a carrier wheel, which itself is designed to support, in addition to the centrifugal forces from the Ti-sectors, also its own centrifugal forces, while minimising its own weight. As explained below, the carrier wheel can be kept at room temperature. Its design is considered as standard engineering, where the centrifugal stresses can readily be kept between 50-100 MPa, while the total weight of the wheel can be kept at well below 50 kg. This will, however, not be considered further in this report, since it can readily be handled by qualified engineering firms.

However, some care has to be taken for the attachment of the Ti-sectors to the carrier wheel, see Figure 2.12. Firstly, the thermal contact must be minimised between these two components, to avoid any increase of average or transient temperatures in the carrier wheel. This prevents any possible unbalances in this fast rotating wheel, like non uniform deformation through thermal expansion. Therefore, thermally isolating ceramic spacers, as shown in Figure 2.12, are foreseen at this interface.

Secondly, the attachments of the Ti-sectors to the carrier wheel must be sufficiently robust to resist to its centrifugal forces at this location. But since the temperatures expected in the Ti-sectors at this interface are of the order of 300 ^{o}C , this can conveniently be achieved by a locking shoulder, as shown in Figure 2.12.

And finally, the attachment of the Ti-sector must be designed such that no thermal expansions of the Ti-sectors are restricted and that it can expand freely in tangential and radial direction. This reduces the thermally induced stresses. As shown in Figure 2.12, this can readily be achieved by allowing the locking shoulder to move tangentially along the groove with respect to the carrier wheel with a single fix point at the middle of its width.

The loads in the Ti-sector through centrifugal forces can readily be estimated. The results are collected in Table 2.3. The maximum radial stress obviously occur at the inner part at the attachment and are about 10 MPa for a rim of 10 cm height and 23 MPa for a larger height of 20 cm, which are completely tolerable at the temperatures of about 300 ^{o}C , as expected at this location. Some open question remain along the centreline, where the centrifugal radial stresses are very low, only about half of those at the inner side, but at however higher temperatures of around 560 ^{o}C .

The thermal stresses, induced by the temperature field inside the thin sector, symmetric around the centre line in Y-direction and about uniform in tangential direction, can be estimated by classical considerations of thermal stresses in free bars. In this condition, only the temperature deviations from the average temperature matter. The results are also given in Table 2.3. Standard average values at room temperature for the Youngfs modulus of 100 GPa and a thermal expansion coefficient of 10^{-5}/K have been applied. Compressive stresses in tangential direction along the centre line of -125 MPa result, while they are of the same value at the boundary, but in tension. In this estimate, however, the weakening of the material at elevated temperatures of about 550 ^{o}C along the centreline is ignored. This requires further computation studies or better, material tests should be performed under these conditions by qualified institutions.

Finally, the pulsed stresses, induced by the adiabatic temperature rise per pulse, which are of the order of 100 MPa, must still be taken into account. These pulsed stresses could in principle lead to fatigue of the Ti, in particular at temperatures between 500-600 ^{o}C , which should also be investigated by dedicated material tests.

The resulting time average stresses are collected in Table 2.3:

Table 2.3: time average stresses

Centrifugal radial stress along the lock at $Y = 0$	10 MPa	At Temperature of 300 ^{o}C
Centrifugal radial stress along centre line at $Y = Y_0$	5 MPa	At Temperature of 550 ^{o}C
Tangential thermal stress along centre line	-125 MPa, in compression	At Temperature of 550 ^{o}C
Tangential thermal stress along boundary	+125 MPa, in tension	At temperature of 300 ^{o}C

2.3.6 Rotation Control and Synchronisation with Slots

Since it is proposed to use Ti-sectors of about 10 cm width, instead of a complete ring, and to allow their free thermal expansion, slots of about 0.2 mm between the sectors should be foreseen, to prevent any contact among neighbouring Ti-sectors. It should also be envisaged to servo control not only the rotation velocity of the wheel, but also its position, to synchronize it with the impact of the beam pulses, spread over one sector and avoiding the slots. This should be possible with up to date servo control processors and adequate sensors, arranged around the axis of the target wheel. It requires however a sufficiently strong coupling of the motor torque to the wheel to arrive at a fast response.

As an example a velocity, deviating from the nominal velocity by 10^{-4}, would rotate the impact pattern around the wheel by a shift of 3.5 mm over a time of 0.35 s and the beam pulse might migrate towards or across a slit.

If such a position control is difficult to implement, one would have to accept that the beam is swept every so often across one slot of 0.2 mm width between two sectors. This will create a small valley in the positron yield by at most 7% over about four sigmas of the bunch rms width of 1.2 mm[30]. This has, however, to be put into perspective with the anyway existing variations of 100 % of the yield at either end of the beam pulse, extending again over a width of about four rms bunch widths. If those variations cannot be tolerated, the front and end slopes as well as the dips due to the slots have to be gated out.

2.3.7 The Magnetic Bearings

Magnetic bearings are commonly used under vacuum for fast rotating wheels, like turbo molecular pumps, Fermi choppers and fly wheels for energy storage. Here, the rotating axis is supported, so to speak gfloatingh in a suitably shaped magnetic field, created by electromagnets or permanent magnets, arranged around the axis. As in contrast to mechanical ball bearings, some small lateral displacements of the lateral position of the axis may occur with magnetic bearings. Such displacements can for example be due to pulsed magnetic friction forces at the rim of the wheel, which are induced by the pulsed flux concentrator. One will have to study if these displacements at the axis are small enough due to the mass inertia and stabilising centrifugal forces of the wheel. Also, servo control of the position of the axis may be possible.

By preliminary information from manufacturers, such devices can also be adapted to the needs of the wheel for the ILC positron target, in terms of weight of the wheel, pulsed loads on it and its radiation resistance. This requires, however, a detailed feasibility study, to be followed by solid prototype tests. This certainly represents a major issue for the forthcoming R&D phase of the wheel, involving adequate funding and manpower.

2.3.8 Outlook and Conclusion

With the reduced average power of 2 kW, deposited in the 7 mm thick Ti-target, the evacuation of the heat by thermal radiation directly through the side faces of the target is possible. The proposed lay out and the cooling can readily be validated on a small, nonrotating sector of the wheel in a simple laboratory set up, with little cost and resources.

Mounting individual target sectors onto a carrier wheel has the additional advantage, that there is no cross talk among neighbouring sectors, while in a full wheel, cross talk can occur through temperature and stress variations around the wheel. Finally, the carrier wheel can be designed to standards in terms of stresses and weight, since it is not influenced by the beam loads in the target. The functionalities of the target sectors and the carrier wheel are distinctly separated, while in a full Ti-wheel the functionalities overlap.

EDMS Nr.: D00000001165115 Rev: B Ver: 3 Status: Released - for publication Dat.: 23. May 2018

The laboratory tests of the fast rotating wheel and its dynamic response to the mechanical and thermal loads are obligatory. This involves the setup of a “one to one scale” prototype, a wheel rotating in vacuum and supported by rotating magnetic bearings. Heat input around the rim of the spinning wheel via infrared or inductive heaters should be possible. Water cooled coolers must therefore be foreseen. Clearly, this requires to set up a detailed R&D plan, extending over several years, and adequate resources for this must be made available in due time.

As shown in the above studies, the Ti-target material, being submitted to elevated temperatures and stresses, may reach its limits at the presently envisaged power deposition of 2 kW or above. This could lead to a limited life time of the wheel. Therefore, studies of alternative target materials, supporting eventually higher input powers, with higher emissivity, mechanical strength and thermal conductivities should still be pursued. High temperature Ni-alloys could be suitable candidates. Also, Copper-Graphite, a mixture of sintered graphite and Cu-powder may be a candidate. It has been used in ancient times in electro motors, where the rotor is fed with current by sliding electrical contacts through such Graphite collectors, with low electrical resistance and submitted to high temperatures and stresses.

2.4 R&D Plan for the Target for Undulator Scheme

The R&D work for the next years comprises the following items:

1 finalize the target studies for a target wheel (250 GeV collision energy)

2 test in the lab the cooling by thermal radiation for a target piece

3 develop a full-size mock-up for the target to test the target rotation in vacuum

Item (1) is obvious. There is no doubt that radiative cooling will work. However, the cooling efficiency depends strongly on the emissivities of the cooler and target materials as well as on geometrical factors.

Tests as suggested in item (2) allow to study the performance also beyond the desired operation temperatures of the target. This is essential for the safety margins and allows improvements of the design.

Item (3) is more complex – it includes the full set-up of the target including motor, bearings and full-size wheel. Preliminary work for such mock-up design can be started in parallel to item (1) and (2) if the manpower is available. The preparation of the full-size mock-up should take into account the results of item (2).

2.4.1 Test of radiative cooling with a target piece

Such test could be done relatively easy: A stationary target piece is positioned in a vacuum chamber and heated; the cooling is arranged by coolers in front of the piece.

The energy deposited in the target by one ILC250 pulse is about 500 J. This corresponds to an average energy deposition in the target area of about 80 W. This heat equivalent must be brought into the top of the target piece, either by ohmic or by inductive heating to achieve a temperature distribution profile similar as in the target wheel. Thermocouples will be installed on target and cooler to test the efficiency of the cooling system. Target piece as well as cooler will be replacable so that a flexible measuring program can be performed. Such program will include the following tests:

EDMS Nr.: D00000001165115 Rev: B Ver: 3 Status: Released - for publication Dat.: 23. May 2018

- The influence of emissivities of target sample and cooler on cooling effiency
- The influence of the geometry. This includes also special shapes with fins in the target piece and cooler.
- The influence of different materials and their connections. In case of high luminosity or later polarization upgrade the energy deposition in the target increases. To avoid overheating in the outer region of the Ti6Al4V disk, the target wheel should consist of a Ti6Al4V target rim which is connected with a radiator made of material of high thermal conductivity (see also Sec.2.3). This allows to extract the heat faster from the target and reduces the maximum temperatures substantially. However, the connection between different materials has to be studied since it must be stable over a wide temperature range if the spinning wheel.

Also the simple set-up requires preparative simulation work in order to design a test module which allows all these measurements up to high temperatures. The material for the walls of the vacuum chamber has to be defined. Only the coolers opposite the target sample should absorb thermal radiation, the other walls should consist of material which hardly absorbs heat. Otherwise the test setup would distort the efficiency of the cooling by radiation. Ohmic heating seems the most simple option to increase the temperature in the target header. Cartridge heaters are available, see for example reference [28]. They stand working temperatures of 760°C (and even higher) and deliver Watt densities up to about $60\,\mathrm{W/cm^2}$.

After designing the test module –which includes the simulations for the temperature distribution in the module for different test options– 1 year work of 1–2 engineers and technicians should be sufficient to finalize the construction drawings, manufacturing and assambly and to perform test runs.

2.4.2 Full-size mock-up to test target rotation in vacuum

A final lab test and the validation of the target wheel are mandatory. The following steps towards a mock-up are necessary:

1. Study of the response of the spinning target wheel to the beam pulses, stress due to transient and average heating and thermal expansions are under way; currently performed at DESY Zeuthen and Universität Hamburg. To finish these studies for all source options expected in the first years of ILC running, a manpower of about 1–2 persons over 1 year is needed.
2. The results of these studies have to be converted into engineering solutions by experienced institutes or companies to prepare drawings and manufacturing of the target wheel. This requires simulations with validated mechanical and electromagnetic FEM codes by qualified persons.
3. Magnetic bearings are recommended; they are widely used and work maintenance-free over long time. Experience exists in Jülich (*e.g.* neutron choppers) or SKF Company (see also talk by M. Fukuda at LCWS 2017). Based on item (2) a performance specification has to be written serving as an input for a feasibility study for the magnetic bearings. It should contain
    - Mechanical layout of the wheel, materials, weight

EDMS Nr.: D00000001165115 Rev: B Ver: 3 Status: Released - for publication Dat.: 23. May 2018

  - all beam and magnetically induced loads in the wheel
  - Static and dynamic imbalances, vibrations
  - Vacuum requirements, outgassing, bake out

4. Design and build a mock-up to perform final lab tests and validation of the wheel:
   - In a first step a reduced model with a small wheel rotating in vacuum could serve to validate the main issues, like magnetic bearings, drive motor, weight.
   - As a second step a full sized wheel with a vacuum tank must be manufactured and tested in the lab.

   The average heating corresponding to ILC beam load could be brought onto the outer rim by inductive or infrared heating. For the details of such beam-substitute heating simulations are necessary to achieve a temperature distribution and cooling conditions that correspond to that of the target wheel in ILC operation. The mock-up allows comprehensive studies of the vacuum conditions as well as thermal and mechanical behavior. Also vibration studies as well as wheel acceleration and deceleration are important. If the target wheel has expansion slots, diagnostic tools are needed to control the rotation frequency. Last but not least, a special housing for the mock-up tests is required to obtain the safety regulations.

Since the positron source must work also at higher energies as well as for higher polarization, further studies are necessary to upgrade the target corresponding to the energy, luminosity and polarization requirements. This work has to be done taking into account undulator parameters etc. No showstopper is seen; the discussion of details is not the goal of this write-up.

2.5 Positron capture for the Undulator Scheme

The TDR (volume 3.I, p.132 and volume 3.II, p.98) gives a brief description of the optical matching device (flux concentrator), which creates a pulsed, solenoidal magnetic field (peak 3.2 Teslas). There are several examples in the past but, for our undulator scheme, the most challenging is the long flat-top pulse up to about 1ms (0.726 ms for 1312 bunches). The TDR gives a design of such a flux concentrator but the effect of skin depth for low frequency was not taken into account. This is decribed here.

The longitudinal slit is responsible for the leakage of the magnetic flux through it and for the appearance of the azimuthal inhomogeneity of the magnetic field, as well as for the displacement of the optical axis of the magnet. In an ideal symmetrical pulsed magnet, when the influence of the slit is neglected, the transverse magnetic field at the magnet axis is equal to zero, i.e. the optical axis of the magnet coincides with the geometrical axis of the conical cavity.

Unfortunately, FC is not an axisymmetric device from eddy current point of view. The narrow slit of the FC body forms such asymmetry and generates a transverse component of magnetic field on the geometrical axis of device. The transverse component has a clearly defined set of odd field harmonics with a strong domination of dipole component. The typical peak value of dipole harmonic averages 3%-4% of a peak longitudinal field with a current pulse duration in 20-30 μs range.

EDMS Nr.: D00000001165115 Rev: B Ver: 3 Status: Released - for publication Dat.: 23. May 2018

The influence of the skin effect in time consists in that all radial dimensions of cavities and narrow slot (responsible for FC electro-magnetic parameters), are larger than its geometrical dimensions, which affects the value and distribution of the magnetic field at a given value of the pulsed magnet current. For example, the skin-layer depth with a typical pulse duration of 7-50 μs and copper body of matching device is about 0.2-0.7 mm and the same value with pulse duration of 1000 μs is already about 3.4 mm, which is comparable with a minimum aperture of a FC.

A typical width of a FC body slit does not exceed 0.2-0.3 mm and is defined by a technological reason of FC manufacturing. In case of skin-layer depth become several times bigger than the FC slit the flux in the slit is comparable with a magnetic flux in its aperture. The leakage of the magnetic field through the slit causes strong azimuthal inhomogeneity of the magnetic field. The deviation of the transverse component distribution from the ideal one becomes much stronger. The optical magnetic axis in such a magnet may be totally absent. This negative situation is typical for a FC with a long pulse in millisecond range, i.e. when the effective size of the slit is comparable with the magnet aperture.

Taking into account a distortion of transverse magnetic field, the problem of field quality is most essential parameter of matching device and one may have a dramatic effect on the positron bunch dynamics and total positron yield. So, high transverse magnetic field component makes the trajectories of positron strongly distorted and as the result, a beam line are not centered with accelerator line well. Generally, the positron yield may rich a maximum at magnetic field strength of 1-2 Tesla and even decreases with a rising up of field strength of matching magnet.

Figure 2.16 shows the profile of the longitudinal field on the axis as functions of the longitudinal position at various time. Figure 2.17 shows the profile of the transverse field as functions of the longitudinal position at various time. The effects of the latter seems quite significant.

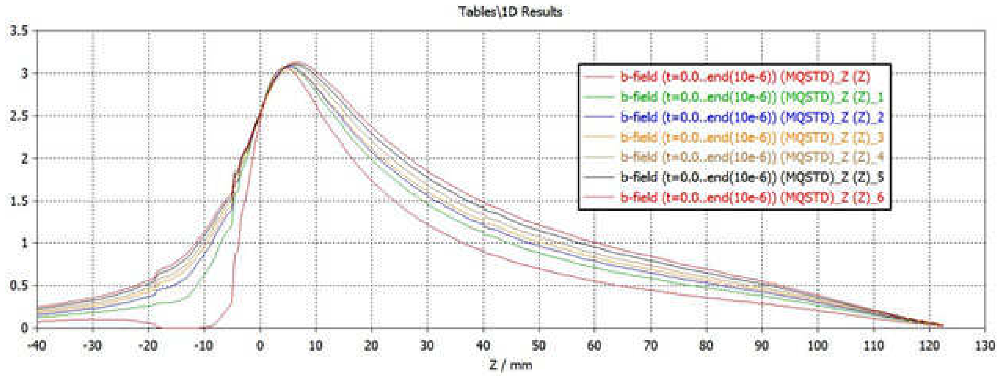

Figure 2.16: Longitudinal field profile [Tesla] at $t=$ 12, 100, 200, 300, 400, 600, 800 μs (red green blue yellow dr-yellow black red)

EDMS Nr.: D00000001165115 Rev: B Ver: 3 Status: Released - for publication Dat.: 23. May 2018

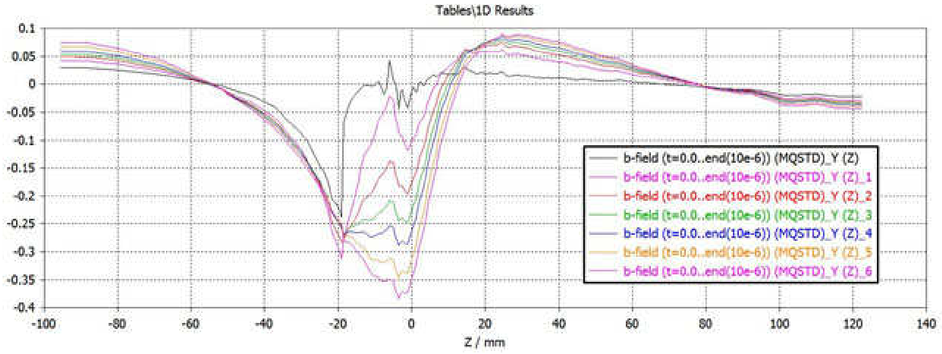

Figure 2.17: Transverse field profile [Tesla] at $t=$ 12, 100, 200, 300, 400, 600, 800 μs (black pink red green blue yellow pink)

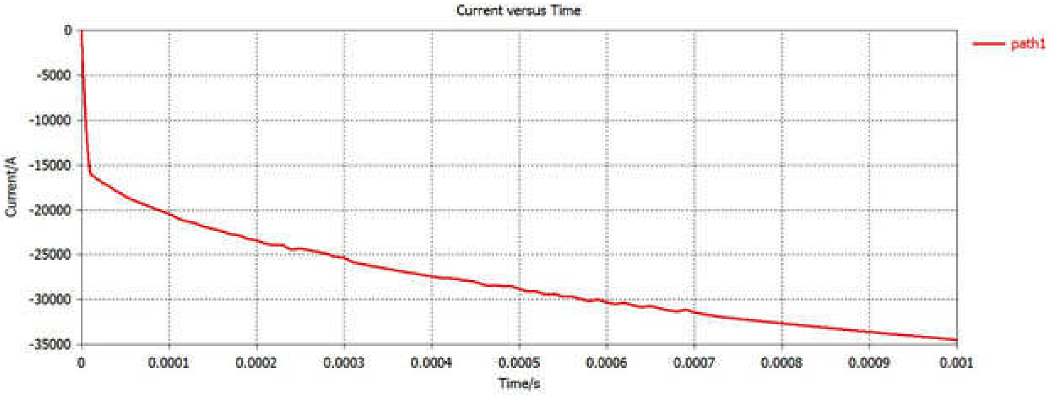

Figure 2.18: Current in the FC as a function of time

EDMS Nr.: D00000001165115 Rev: B Ver: 3 Status: Released - for publication Dat.: 23. May 2018

2.6 Photon Dump

2.6.1 Introduction

Following the design of the water dumps for the main e$^-$ and e$^+$ beams of the ILC with a maximum power 17 MW, it is obvious to adopt this line of thought also for the design of the dump of the photon beam. This narrow photon beam with a cross section of below 2 mm is created in the Undulator with an average power of 120 kW for the 250 GeV high lumi case and 108 kW for the 500 GeV high lumi case ([35]). It hits the 7 mm thick Ti-target, where however only a small amount of the beam power is absorbed.

Therefore permanent dumping of the full photon beam power is required during operation. In contrast to the main water dumps, the photon beam cannot be swept magnetically across the front face of the dump to reduce the energy deposition density PEDD in the material of the dump. However, when also water is used as the dumping material, as considered in the TDR, it should be pressurised to about 12 atm, in order to prevent temporary boiling during or at the end of each pulse. As a consequence, a 1mm thick Ti-window would be required to resist to such pressures. In more detailed studies it appeared however, that such a thick window would suffer from fatigue through high thermal cycles during each pulse and severe radiation damage. Therefore, a different approach has been proposed ([36]), in particular for the design of the beam window, separating the beam vacuum from the water.

As an alternative, also the use of Graphite for the dump, tolerating high temperatures, might also be envisaged. This is also being studied within this Working Group ([37]). The method uses Graphite plate on copper, having a shallow angle with the photon beam to reduce the heat/PEDD. The study is still in an initial stage so that it is not described in this report.

2.6.2 The Beam Window

Thin foils or disks of a high temperature Ti-alloy, TiAl4V, are readily available from industry and commonly used for beam windows. As an alternative, Beryllium windows could be an option, but this is not considered here at this stage.

The critical issue is now to calculate the PEDD of the narrow photon beam in the window. This has been done with the FLUKA-code in an initial study ([36]) and is reviewed here, also including the recently updated beam parameters.

During the discussions within the Positron Source Working Group, it seems possible to place the window and the dump at a distance of 2000 m from the target. There due to the divergence of the photon beam, acceptable beam sizes, temperature rises per pulse and stresses are attained. The results for the PEDD in Ti-windows vrs. the window thickness are shown in Figure 2.19, illustrating the strong dependence of the PEDD on the beam cross section at the close (48 m from the target) and the far (2000 m) beam dump.

There is a space in the present design of the Beam Delivery System to accomodate a long photon beam pipe. The choice of 2km is somewhat arbitary but, then, the photon dump is close to the positron main dump so that there is a possibility to share some of the equipment such as water cycle system.

The relevant pulse by pulse effects are collected in Table 2.4 for the close and far dump for various window thicknesses.

EDMS Nr.: D00000001165115 Rev: B Ver: 3 Status: Released - for publication Dat.: 23. May 2018

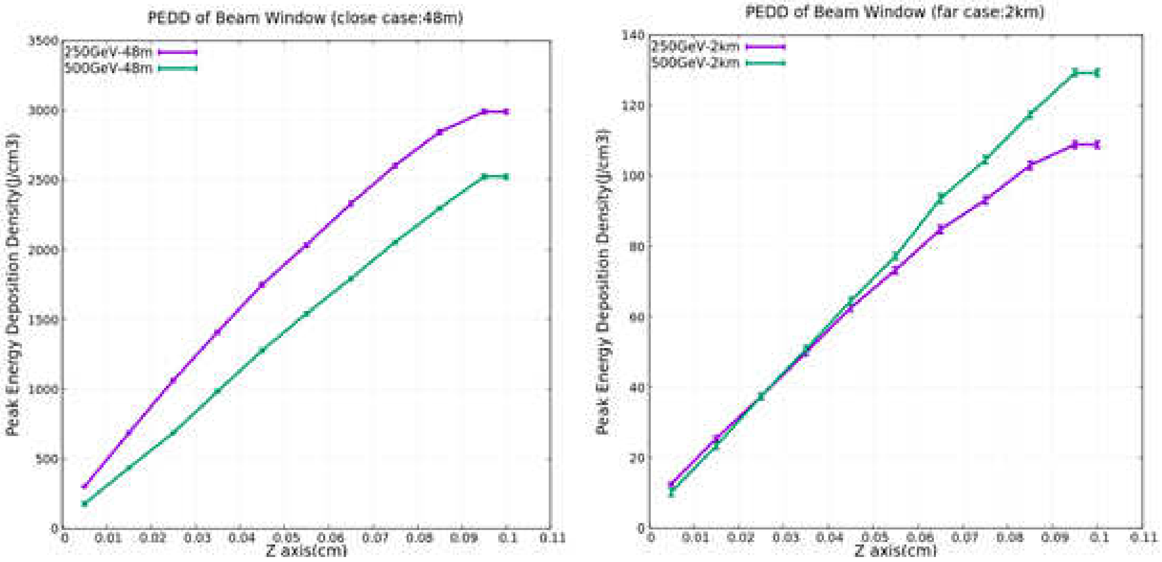

Figure 2.19: Peak energy deposition density PEDD vrs. window thickness at the location of the window at 48 m (left) and at 2000 m (right) from the target. Watch the different scales on the left and the right figures for the two cases.

Table 2.4: Pulse by pulse effects, temperature rise ΔT/pulse and thermally induced stress σ, for the high lumi cases in Ti-windows for various thicknesses for the close and far windows.

Beam Conditions	Window thickness (mm)	0.1	0.2	0.3	0.4
250 GeV-48 m	PEDD(J/g)	113.3	198.1	280.3	358.5
	ΔT/pulse(K)	227.	396.	560.	717.
	σ(MPa)	340.	594.	840.	1076.
250 GeV-2000 m	PEDD(J/g)	4.3	7.2	9.9	12.7
	ΔT/pulse(K)	8.6	14.4	19.8	25.4
	σ(MPa)	12.9	21.6	29.7	38.1
500 GeV-48 m	PEDD(J/g)	68.8	127.5	189.6	254.1
	ΔT/pulse(K)	137.6	255.	379.	508.
	σ(MPa)	206.	383.	569.	762.
500 GeV-2000 m	PEDD(J/g)	3.7	6.9	9.9	13.1
	ΔT/pulse(K)	7.4	13.8	19.8	26.2
	σ(MPa)	11.	21.	30.	39.

EDMS Nr.: D00000001165115 Rev: B Ver: 3 Status: Released - for publication Dat.: 23. May 2018

As clearly demonstrated in this table, the windows for the close dump will suffer from high temperature rises and thermal stresses, which will lead to a very short lifetimes. To the contrary, the values achieved for the far dump become very acceptable.

In addition to the above presented short term, pulse by pulse effects in the window, accumulative effects like the evacuation of the average power and cooling as well as radiation damage have to be considered.

As illustrated in Figure 2.20, a double walled Ti-window is proposed, which is cooled by He-gas flowing between the two sheets in a closed circuit. The He-gas is guided via nozzles along the inner surfaces of the heated regions of each of the two Ti-windows. Cooling is achieved with a He-flow at slightly above atmospheric pressure and a velocity of at most 100 m/s. This gives rise to a strongly turbulent gas flow (the Reynolds Number is about 10^4) but is still far away from the supersonic regime. This results in a forced convection coefficient, extracted from standard engineering tables, of around 0.13 W/cm^2/K and in a He-flow of 0.02 kg/s. In a more detailed FEM study, a convection coefficient of 0.09 W/cm^2/K was achieved.

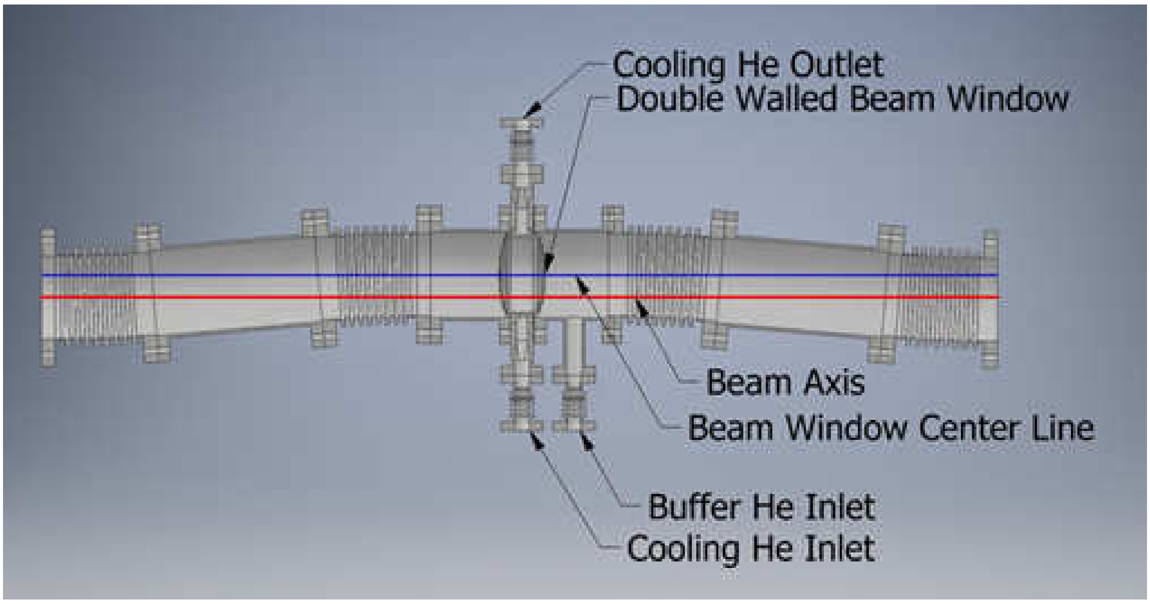

Figure 2.20: Layout of the double walled, He-cooled window. Through the bellows system the central unit can be displaced simultaneously in horizontal and vertical direction (the driving system is not shown here). The beam (the red line) is thus hitting the window displaced from its central line (blue line), describing a circle around its centre. In this way a tumbling movement is created.

The windows have, as shown in Figure 2.20, a spherical shape to provide maximum resistance against static gas pressure. With a diameter of the window of about 15 cm, long axis, and a depth of the calotte of about 2 cm, short axis, such a window with a thickness of 0.2 mm will even stand a gas pressure of 2 Atm. This will create a stress of about 70 MPa, well below the elastic limit of the Ti-alloy of 400 MPa. Manufacturing of spherical thin sheets by hydro pressure forming is a well established technique in industry.

Although the temperature rises per pulse are low, cumulative effects, like the pile up of temperatures after many pulses in the steady state, it is of importance to spread the pulses over a larger area at the window. This would also reduce the risk of failure due to

EDMS Nr.: D00000001165115 Rev: B Ver: 3 Status: Released - for publication Dat.: 23. May 2018

repeated thermal stresses, 90 million. pulses over 5000 h of operation, and accumulation of radiation damage, dpa, over such duration of operation. Such a spread of the beam impacts over the window can be achieved by a displacement of the window unit via a bellows system in horizontal and vertical direction, as shown in Figure 2.20. To create this displacement, the tumbling movement of the window, a synchronised sinusoidal displacement in horizontal as well as in vertical direction of the central window unit via a bellows system is required. In this way the beam impacts are spread around a circle. Here a tumbling radius ρ of 3 cm is chosen. To avoid pile up of successive beam pulses, a displacement of at most 2 cm between the pulses at 5 Hz, a tumbling velocity of 2.0 cm/200 ms, i.e. 0.10 m/s is required, resulting in a rotation frequency of 0.53 Hz or 1.9 s/turn. As compared to a stationary window, in this tumbling window the pulses are spread over a surface enlarged by a factor of 9.5. The acceleration required for the lateral tumbling movements with the necessary velocity is only 0.33 m/s^2, well below acceleration by gravity of 10 m/s^2. Thus, the loads in the drive mechanics should be small. Clearly, some flexibility in the inlet and outlet pipes is required to allow for the movement of the central unit (see Figure 2.20).

In Table 2.5 the peak temperatures at the end of each pulse are given, once a stable temperature cycling is reached. With the assumed parameters for the He-cooling, as given above, the cooling time constant of the exponential temperature decay after each pulse is below 1 s. Since this is smaller than the repetition time of about 2 s between pulses around the tumbling window, the temperatures will cycle close to room temperature, i.e. the inlet temperature of the He-gas. This clearly demonstrates the advantage to spread the average power, deposited in the window, over a larger area and facilitates the cooling. Moreover the radiation damage, a critical issue for stationary windows, is given in terms of dpa also for the tumbling window in Table 2.5. According to computations with FLUKA, the dpa seems to be rather constant along the thickness of the thin Ti-windows. To define the life time of the window, a maximum allowed dpa of 0.5 is assumed.

Table 2.5: The pulsed peak temperatures above room temperature (inlet temperature of the He-gas at 20 ^{o}C) and the average power, to be removed from each tumbling window with a thickness d are given for the far dump. For the He-gas cooling, see the text. For the life time of the windows, a maximum limit of 0.5 dpa is assumed.

Beam Conditions	250 GeV	250 GeV	500 GeV	500 GeV
Dump location	close	far	close	far
Window thickness d (mm)	0.2	0.4	0.2	0.4
Peak Temperature (^{o}C)	34.5	48.5	34.	49.3
Av. Power (W)	16.2	43.3	3.9	10.9
Dpa/5000h	0.25	0.25	0.71	0.71
Lifetime (h)	10,000	10,000	3,600	3,600

As also shown in Figure 2.20, a gas buffer volume is created in the downstream space between the window and the water dump by injecting He-gas at this location. This prevents a direct contact of the Ti-window with the water of the dump (see later), which avoids detrimental radiochemical and corrosive attacks on the Ti-material in contact with air or water vapour.

EDMS Nr.: D00000001165115 Rev: B Ver: 3 Status: Released - for publication Dat.: 23. May 2018

2.6.3 The Water Dump

In Figure 2.21. the peak energy deposition density PEDD in the water per pulse is given vrs. z, the beam direction for the close and the far dump. From this the adiabatic temperature rises per pulse at the front face at z=0 and along the "hottest" z-position between z=5.-10. cm are collected in Table 2.6. In contrast to earlier studies with smaller beams and a dump close to the target, here now at a distance of 2000 m, boiling can be excluded without pressurising the water.

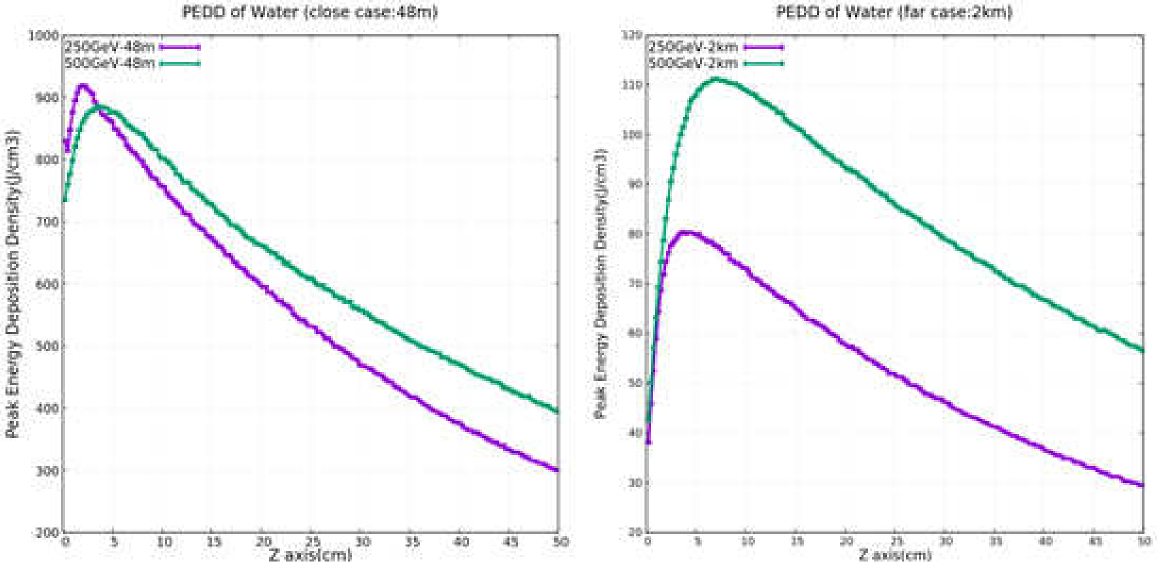

Figure 2.21: The energy deposition density per pulse in water are shown for different beam scenarios vrs. the beam direction z. Watch the different scales for the close and the far dump.

Table 2.6: Adiabatic temperature rises in the water dump per pulse at different z-locations.

	500 GeV close dump	250 GeV close dump	500 GeV far dump	250 GeV far dump
ΔT/pulse (K) at z=0	174.	190.	12.	12.
ΔT/pulse (K) at z=5-10 cm	210.	219.	26.5	19.1

Some small, residual pressure variations, positive as well as negative, may still be created by the beam pulses. The rise times of the temperature and thermal expansion in the water, caused by the beam pulse of 1 ms duration, will put the heated water volume into motion. This can cause small pressure variations, positive as well as negative. In contrast to pulses with micro-s duration, at which rapid pressure bumps and acoustic waves can be created, no massive pressure waves are therefore expected in this milli-s regime. But this should be confirmed by FEM-computations.

Finally, rapid formation of bubbles during the pulse could be caused by gas, dissolved in the water and be released rapidly by pressure variations. If such effects with a temporary reduction of the water density during the pulse occur, it just means that additional depth of water will be required, which is sufficient till all the energy dissipated in this reaction channel is consumed.

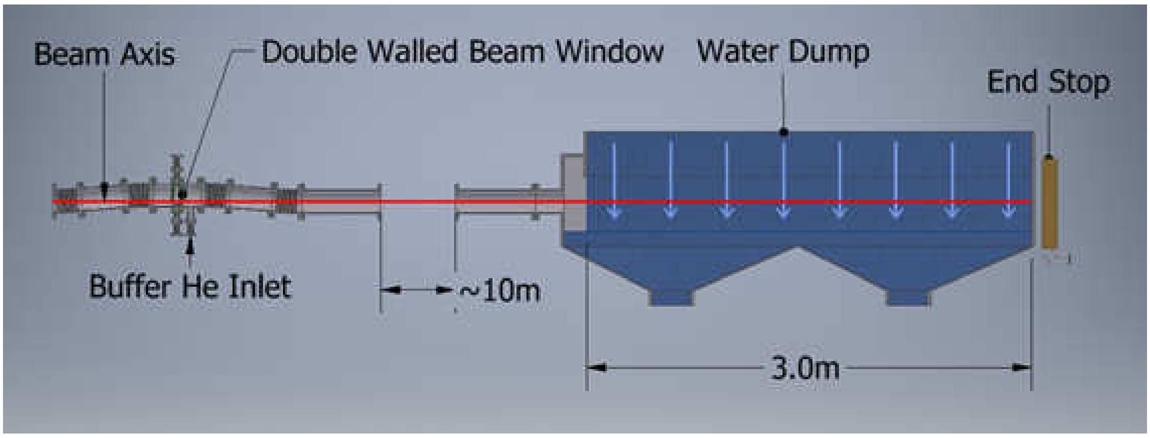

Figure 2.22: Layout of the water dump. It shows the upstream entrance beam pipe, through which also the buffer gas from the window flows into the water volume and the actual tank, which contains the vertical flow of water, kept free at its upstream front face. The final end stop, absorbing the remaining energy after the water depth of 3.0 m, is also indicated in yellow.

Figure 2.22 shows a sketch of the water dump and its container. With a small water velocity in vertical direction of only 0.1 m/s, absolutely laminar, a displacement of the dumping material by 2 cm between the time of two pulses of 200 ms should be adequate. In this way little pile up of heated water between pulses will occur. Assuming tentatively a length of the water volume of 3.0 m and a horizontal width of the water stream of 10 cm, a flow of 30 kg/s is required. This water stream absorbs an average beam power of up to 100 kW, about 80% of the total beam power.

The length of the water dump has to be chosen sufficiently long so that at its end the PEDD in the downstream wall of the water tank and in the additional downstream end stop, possibly in copper, is sufficiently low. The maximum PEDD of about 3.0 J/g is reached at this location for the 500 GeV-case, which is well tolerable for stainless steel for the tank as well as for the end stop in copper, which is placed outside the water tank. Thus a total length of the water tank of 3.0 m should provide sufficient safety margin. Since the average power, deposited in the end stop with a thickness of 10 cm is still of the order of one kW, some cooling of the end stop should be foreseen.

A free falling water curtain, see Figure 2.22, or vertically flowing water, firmly confined laterally by both side walls of the tank, are possible. In the latter case however, some pressure bumps at the side walls of the water container and vibrations may be caused there.

The He-buffer gas may be recuperated in an outgassing tank. Such equipment must be foreseen in any case in the water treatment plant, to clean the water, to control its pH-value and its electrical resistivity and finally to de-ionise it, also to eliminate Tritium and Be^7. Finally, to place the photon dump in the vicinity of the water plant of the main ILC dumps, will be advantageous, since it can be considered as a small annex to the much larger infrastructure for the main dumps.

2.6.4 Operational Aspects

Considering now the operation of the water dump, the risk of accidents and water leaks are minimal and consistent with or even better as compared to other installations of similar nature at low pressure. In any case, safety rules will require a safety sump, a tank capable to retain any water which may leak out from the dump.

Radiation issues are well controlled. The main activity will be concentrated inside the water treatment plant and not at the dump. The activity in the water is diluted by the much larger total volume of the circuit and the "hottest" points are probably the ion exchangers. However, some contamination of the tank walls and the piping may still persist, even when the water has been drained. But experience in accelerators and around neutron spallation sources exists.

Concerning the tumbling window, its position at about 10 m upstream of the dump should allow easy human access, possibly with some additional shielding in the space in between. Still, it represents an "active" component, like the moving bellows and the tumbling mechanics, which requires regular maintenance.

Of course, also the windows may have to be replaced regularly or can even fail during operation. Some special tooling for ease of handling and precautions to protect personnel should be foreseen. However, mechanical fatigue or radiation damage will, in general, occur gradually and defects will be recognised in due time by a slow loss of vacuum. In any case, fast shutter valves must be foreseen on either side of the tumbling window, to prevent a massive and sudden influx of air.

The lateral beam position upstream of the dump should be measured on a pulse by pulse basis, since in case of large lateral drifts of the beam the window frames and the beam pipe can be damaged. This sensor should then create an interlock signal to stop the beam. To protect further the dump system against fatal accidents, like a very fast displacement of a single pulse, a sacrificial collimator could be installed upstream of the system. This collimator could possibly be made of graphite with an appropriate aperture, to protect all critical downstream items.

2.6.5 Discussion of Optional Simplified Versions of the Window and Water Dump

As has been shown above, by placing the window and the dump at a distance of 2000 m from the target, where the beam cross section is enlarged to about 1.8 mm, a reliable dumping system with very conservative design values can be conceived. To put this into perspective with possibly more simplified and less complicated systems for the far dump, in the following, some alternative aspects are discussed.

One possible simplification could consist in using a He-cooled double walled, but static Ti-window, without tumbling. The pulse by pulse values are of course the same as quoted in Table 2.4. The accumulative effects, like the piled up peak temperatures during stable cycling and the lifetime for a maximum dpa of 0.5 are quoted in Table 2.7.

From the above considerations one may conclude that, although the average temperatures could be acceptable, the life time due to radiation damage will be rather limited and well below the envisaged life time of 5000 h, corresponding to one year of operation.

Finally, a layout is considered where now a static Ti-window is mounted directly onto the water tank, in contact with the front face of the water. As has been shown, the temperature rises in the water per pulse are well below the boiling point and therefore

EDMS Nr.: D00000001165115 Rev: B Ver: 3 Status: Released - for publication Dat.: 23. May 2018

Table 2.7: Peak temperatures during stable cycling and lifetimes for maximum of 0.5 dpa are given for a stationary, non tumbling window.

Beam Conditions	250 GeV	250 GeV	500 GeV	500 GeV
Window thickness (mm)	0.2	0.4	0.2	0.4
Peak temperatures (^{o}C)	60.	147.	58.4	151.
Life time (h)	1000.	1000.	352.	352.

the pressure in the water can be kept at 1 atm. Taking again into account the large beam cross section at the far position, the pulsed temperature rises and thermal stresses per pulse in the window are of course again the same as in the above considered layout with tumbling (see Table 2.4).

However now, the window will be stationary and could conveniently be cooled by a dedicated water stream, created through a nozzle along the downstream side of the window inside the water tank. Since water is a very efficient cooling medium, the temperature just before a pulse will be very close to that of the water, little pile up during the steady pulsing will occur. Peak temperatures of 35 ^{o}C and 50 ^{o}C will be reached for window thicknesses of 0.2 mm and 0.4 mm respectively. Also for this situation, the limiting factor is again the life time due to radiation damage, the same as given in Table 2.7.

It appears from the above consideration of some simplifications of the system, radiation damage and thus life time is the main issue. This would entail frequent preventive maintenance and exchanges of the windows. In particular the latter case will be highly critical, if the window, mounted directly onto the water tank and suffering from fatigue and corrosive and radiochemical effects, has to be frequently exchanged.

2.6.6 Conclusion

Since for the photon beam it is not possible, like for the e$^-$ and e$^+$ beams, to spread the beam across the dump to reduce the PEDD, the dump material as well as the window have to move. This is readily achieved by a slow vertical flow of water in combination with a quasi rotating, a tumbling window. Thus, sufficient lifetime of all components will be reached.

For water, in contrast to solid, fixed dumps, "radiation damage" in the dumping material is virtually non existing, since the water is continually decontaminated and reconditioned. If the water resists to one single beam pulse, it will survive very many pulses. It requires however a dedicated water treatment plant, but remote from the dump area, with however non negligible cost. If possible, this dump should be placed at a distance of 2000 m from the target, where the beam cross section is comfortably large to achieve tolerable energy depositions PEDD, without risk of temporary boiling. At this far position of the dump one can combine its water treatment plant with that of the main dumps. Still, the water tank and the end stop will be activated and some radiation shielding will be necessary and safe access scenarios, like also for the main dumps, have to be defined.

For the far dump it requires however that the electron beam and its angular direction, emitting photons in the forward direction, is very tightly controlled all along its path along the inside of the undulator ([5]). To achieve a precision of the lateral position of the photon beam of about 1 cm at the location of the dump at 2000 m, a pointing direction of below 5 μrad is necessary.

The tumbling window, placed by about 10 m well upstream of the dump area, is designed for long lifetime. However, easy access and preventive maintenance during regular shut downs can be foreseen at this location.

However, since the thin windows are submitted to pulsed heating with temperature fields inside the thin foils with strong gradients in radial as well as in axial z-directions, rather complex static and time varying thermal stresses are created. These quasi-static or dynamic loads in such thin membranes could eventually lead to material fatigue, involving buckling and vibrations. All these effects, in combination with radiation damage, are difficult to assess reliably by FEM methods. Therefore window tests with beam should be foreseen, to assess their resistance and lifetime under conditions as close as possible to those of the ILC.

Clearly, the solution with a tumbling window and a free floating water stream with no physical contact with the window, represents the most reliable solution. A stripped down version with a stationary window and possibly mounted directly onto the water container could eventually be possible. However, the additional R&D, necessary for the most reliable solution is minimal, and the physical layout is essentially the same as compared to the stripped down version. Therefore it is suggested to implement right from the beginning the proposed most reliable concept, since in the very hostile environment around the beam dumps it will become increasingly difficult and costly to upgrade a simple version at a later stage towards a more reliable version after operation has been started.

EDMS Nr.: D00000001165115 Rev: B Ver: 3 Status: Released - for publication Dat.: 23. May 2018

Chapter 3

e-Driven Scheme

3.1 System overview

3.1.1 Overview

E-Driven ILC positron source generates positron with the conventional method; 3.0 GeV electron beam impinges on a W-Re target. The configuration is schematically shown in Figure 3.1. The driver electron linac is composed from a S-band photo-cathode RF Gun and 3.0 m S-band traveling wave accelerators. The target is 16 mm thickness W-Re rotating with 5.0 m/s tangential speed. FC (Flux Concentrator) for AMD (Adiabatic Matching Device) followed by 1.3m L-band standing wave accelerators with 0.5 Tesla solenoid field. Chicane removes electrons. The positron booster is composed from 2.0 m L-and and 2.0 m S-band traveling wave accelerators. ECS is composed from 2.0 m L-band traveling wave accelerators with chicanes.

In E-Driven ILC positron source, the positrons for one ML (Main Linac) pulse (1312 bunches) is generated in 64 ms instead of 1 ms. The positron is generated in 20 pulses which contains 66 bunches as shown in Figure3.2. The heat load on the target is much relaxed comparing to 1 ms pulse format with this pulse structure, because only the heat of 66 bunches is accumulated, instead of 1312 bunches. The generated positron is stored in DR for 136 ms which is enough for the radiation damping, and sent to ML and IP[38]. The pulse format shown in Figure3.1 is identical to a part of the DR fill pattern. In this configuration, the generated positron is injected to DR with a nominal kicker which has a long flattop with $0.5\mu s$ and repeated 20 times with 3.3 ms interval. Depending on the DR fill pattern[39], the beam structure is should be matched.

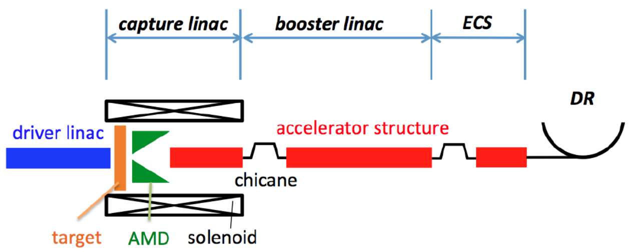

Figure 3.1: Configuration of E-Driven ILC positron source is schematically shown.

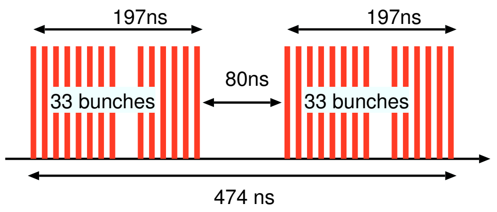

Figure 3.2: The beam structure in the positron source for the 39 mini-train case. Each mini-train contains 33 bunches. Each pulses contain 2 or 1 mini-trains.

Positrons within the DR dynamic aperture[40] is finally captured and sent to IP through ML. Therefore, the positron yield Y_{e+} is defined as ratio of the number of positrons in DR dynamic aperture and the number of injected electrons to the target. To fulfill the required number of positrons at IP (3.2nC/bunch), the yield has to satisfy

$$N_{e-}Y_{e+} > 2.0 \times 10^{10} \times 1.5, \tag{3.1}$$

the factor 1.5 is the safety margin.

A first simulation for the injector part is made by T. Omori [38]. A simulation with the tracking down to DR was made by Y. Seimiya[41] , but no beam loading effect was accounted. A new simulation with the beam-loading effect was done by Kuriki and Nagoshi[42] giving Y_{e+} =2.1.

There are simulations giving a bit different results depending on the detail of the beam line design, treatment for the transient beam loading, etc. An example is found in page 8 of [43] (in Japanese), which gives 1.57.

Assuming Y_{e+} =2.0, 4.8 nC positron in DR bucket is realized with 2.4 nC drive electron intensity. PEDD (Peak Energy Deposition Density) at target was 17.2 J/g[57][44] which should compared with 35 J/g which is a practical limit on the target[45].

In the following sections, we describes the sub-systems with the simulation results.

3.1.2 Configuration of Electron Driver

Electron driver energy is 3.0 GeV and the beam format is identical to that of positron. To achieve 3.0×10^{10} positron per bunch in DR acceptance, the electron bunch intensity is 1.5×10^{10} by assuming the yield 2.0 giving the beam loading current 0.39 A. 3m S-band TW accelerators [46] are employed for the acceleration.

One RF unit is composed from two 80 MW klystrons and four structures. RF power from one klystron is divided to four and one RF line from each klystron drives one accelerator; One accelerator is driven by two RF lines. By changing the relative RF phase for these two klystrons in a pulse, AM (Amplitude Modulation) for the accelerator [47][42] is implemented to compensated the transient beam loading effect. By assuming 10% power loss by WG (Wave Guide), input RF power to one structure is 36.0 MW. The acceleration voltage with 0.39 A beam loading is 50.1 MV[48]. To accelerate up to 3.0 GeV, we need 60 RF structures plus 4 as spare. The number of RF unit is 16 (32 klystrons + modulators and 64 accelerators). The lattice is 4Q+2S (8.0 m) for the first 6 cells and 4Q + 4S (14.4 m) for the last 13 cells. Including 10 m for the injector part (RF gun, bunching, and matching), the total length is 255.2 m.

3.1.3 Target and Capture RF Configuration

The target is 16 mm thickness W-Re alloy. PEDD (Peak Energy Deposition Density) with 66 bunches of electron beam (2.4nC/bunch) is expected to be 17.2 J/g[57]. To avoid any target damage, a rotation giving 5 m/s tangential speed is required. A water-cooled rotating target was designed by T. Omori and M. Yamakata[49]. The detail is presented in Sec.3.6.

For the positron capture linac, we employ the standing wave L-band structure developed for the undulator positron source[50]. The voltage and its variation in a pulse by the transient beam loading effect is evaluated with a multi-cell model by M. Kuriki[51]. The model analyzes the power flow from the wave guide to and between the cells of the

EDMS Nr.: D00000001165115 Rev: B Ver: 3 Status: Released - for publication Dat.: 23. May 2018

structure to evaluate the transient beam loading effect. The boundary condition between the cells is not fully satisfied to simplify the model. Additional studies are required to evaluate the accuracy of the model, or develop a more accurate model.

As same as the electron driver linac, one RF unit is composed from two L-band klystrons and four accelerators. The power of a klystron is 50 MW. Accounting 10% WG loss, the effective input power for one accelerator is 22.5 MW. In the capture linac, the beam loading current is dynamically varied by bunching and particle loss. It is between 1.5 to 1.8 A, except in the first accelerator where it is almost zero[52]. In the simulation, the accelerator voltage is determined according to the beam loading current for each cavity[48]. The average current over the capture linac is slightly lower than 1.5 A giving 10.36 MV/tube acceleration.

According to the simulation[52], the configuration is determined as 9 units (18 klystrons and 36 accelerators). One unit length is 6.00 m giving the total length of the capture linac is 54 m.

After the capture linac, the beam passes through a chicane section to remove electrons, photons, and positron with a large energy deviation. The beam dump for electrons and photons is placed at the same place. A beam collimator is placed in the middle of the chicane to limit the positrons. The chicane section has 8.65 m length designed by Seimiya[41].

The length of target section is 0.35 m. The length of this section (from target to the exit of chicane) is 63 m.

3.2 Configuration of Positron Booster

The positron booster accelerates the positron up to 5 GeV. It consists from FODO cells with L-band and S-band traveling wave accelerators. We employ 2 m L-band and S-band structures designed by Matsumoto[53][54] for Super KEKB. One RF unit consists from two klystrons (50 MW for L-band and 80 MW for S-band) and 4 accelerators. Two RF outputs from each klystron drives each accelerator to compensate the transient beam loading with the RF AM. As same as that in the capture RF, AM is made by phase-modulation of the two RF inputs.

With AM technique, the energy deviation in the pulse by the transient beam loading can be compensated theoretically, but the acceleration gradient is limited, because it requires a high peak power. If the peak power is less than the requirement for the perfect compensation, the energy deviation is appeared. The energy deviation and the acceleration gradient are in trade-off. If 1% energy deviation (in RMS) is acceptable, the acceleration voltage per tube is 17.4 ± 0.2MV for L-band and 25.5 ± 0.2 MV for S-band. 10% power by WG is assumed.

According to the lattice designed by Seimiya[41], a section for four quads is 1.6 m length, the accelerator is 2 m length, and intersection is 0.2 m. Table3.1 summarizes the positron booster configuration. More Q density in the upstream and less density in the downstream to prevent particle loss. The total length of the booster is estimated as shown in Table 3.1, 684.8 m.

EDMS Nr.: D00000001165115 Rev: B Ver: 3 Status: Released - for publication Dat.: 23. May 2018

Lattice config.	N. of cells	Acc. energy	Energy at the exit	cell length	section length
4Q + 1L	14	243 MeV	493 MeV	3.8 m	53.2 m
4Q + 2L	29	1009 MeV	1502 MeV	6.0 m	174 m
4Q + 4L	18	1252 MeV	2754 MeV	10.4 m	187.2 m
4Q + 4S	26	2345 MeV	5099 MeV	10.4 m	270.4 m

Table 3.1: Booster configuration.

3.3 Configuration of Energy Compressor Section

Energy Compressor System rotates the particles in $z - \delta$ phase space by 90 degree. Since the particle distribution after the booster has larger energy spread and smaller bunch length than those for DR acceptance, ECS recovers the positron yield by optimizing the phase space distribution to DR acceptance. The required voltage for ECS is $eV \sim 153MeV$. We employ the 3 m L-band TW structure giving 38 MV with 22.5 MW input with zero beam loading current. 4 tubes are enough to provide the required voltage for ECS. On the other hand, the beam loading voltage is induced. The phase of the beam loading mode is shifted by $\pi/2$ comparing to RF for modulation. The effect of the beam loading can be suppressed by operating a RF unit with the same phase as the beam loading mode, but the opposite sign (acceleration). The amplitude of the RF for compensation should be gradually increased in a pulse as the beam loading amplitude increased.

ECS consists from 3 chicanes (18.6 m, totally 55.8 m) and 4 L-band TW structures (4Q+4L lattice, 22.4 m) driven by two L-band klystrons, and 2 L-band TW structure (2L, 6.4 m) driven by one L-band klystron for beam loading compensation. The section length is 78.2 m.

3.4 Scale of E-Driven ILC positron source and system arrangement

We summarize the estimated section length as shown in Fig. 3.3. The electron driver is 255.2 m . For the positron linac, the target and AMD is 0.35 m, the capture linac is 54 m, chicane is 8.65 m, the booster is 684.8 m, and ECS is 78.2 m. The total length of the positron linac is 826 m. The total length from the electron driver to the positron ECS is 1081.2 m.

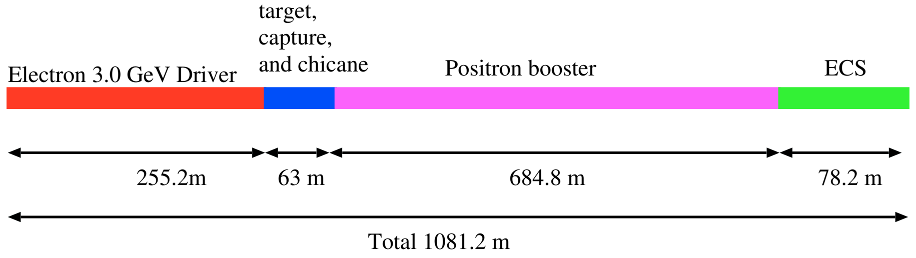

Figure 3.3: The length of the E-Driven ILC positron source based on the current configuration. The total length is 1081.2 m.

EDMS Nr.: D00000001165115 Rev: B Ver: 3 Status: Released - for publication Dat.: 23. May 2018

The system wide arrangement of E-Driven is shown in Fig. 3.4. The electron BDS tunnel has 3490 m, but this length is not necessary for E-Driven positron source. The electron BDS can be same as the positron BDS, 2360 m, because it is enough to accommodate E-Driven positron source. The system upgrade for positron polarization is possible by introducing Undulator positron source as a major upgrade. ML tunnel should be extended with 1640 m that includes 1130 m for Undulator space, 340 m for the timing adjustement, and 170 m for longer ML to recover 3 GeV energy loss by Undulator radiation. The electron arm length (from IP to the end of the electron arm) is 9.24 km for E-Driven case and 10.88 km for Undulator case. In the upgrade from E-Driven to Undulator, the positron arm should be also extented with 0.43 km. As shown in Fig. 3.4, the total length of ILC based on E-Driven system is 18.48 km which is 2.07 km shorter than that based on Undulator system, 20.55 km total.

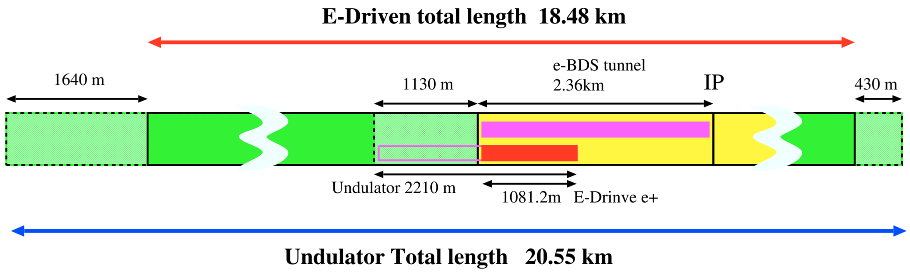

Figure 3.4: A possible system arrangement of E-Driven positron source. The whole system has 1081.2 m in length and it can be accommodated in the electron BDS tunnel which is 1130 m shorter than that for Undulator case. To upgrade Undulator positron source, ML tunnel should be extended with 1640 m in electron arm and 430 m in positron arm. The total length is 2.07 km shorter for E-driven than that for Undulator.

3.4.1 Cooling Water Capability

The cooling water removes heat from devices such as Klystrons, RF structure, Wave guide, RF load, etc. Here, we estimate the water cooling amount for RF structure including the RF load. The fed RF power to the RF structure is not only consumed as heat deposition in the structure and load, but also the beam acceleration. Therefore, the required cooling power depends on the beam current, but we estimated the cooling power with 0 beam current as the maximum.

The required cooling water capability is determined with the cooling power and the allowed temperature variation. Usually, it is 0.1 K for RF structure (cavity), but it can be 10 K by introducing the counter-flow scheme[55]. The required cooling water V[l/min] is estimated as

$$V[\mathrm{l/min}] = \frac{60P[\mathrm{kw}]}{4.2\Delta T}, \tag{3.2}$$

where P[kW] is dissipated power, ΔT is allowed temperature variation. ΔT is 10 K for the accelerator (cavity) and 11 K for RF load. Cooling water for klystron and modulator is not included in the calculation.

Please note that the input water temperature has to be $\Delta T/2$ less than the target temperature, because the object temperature is determined by the average of input and output water temperature. If the target temperature is T_0, the input water temperature is $T_0 - \Delta T/2$. If the heat load P is varied, we have to change the flow rate V according to Eq.(3.2) or temperature as

$$T_{in} = T_0 - \frac{30P[\mathrm{kw}]}{4.2V(l/min)}. \tag{3.3}$$

Table 3.2: Expected heat load on accelerator tube P_{acc} and RF load P_{load} for 1.27 m L-band Standing Wave structure with 22.5 MW RF power. The water cooling amount (l/min) is estimated by assuming 10 K and 11 K temperature variation for the accelerator and load.

Component	$P(kW)$	V (l/min)	N. of unit	total (l/min)
L-band SW cavity	2.84	4.05	36	146
L-band SW load	5.49	7.13	36	257
L-band TW cavity	1.68	2.41	144	347
L-band TW load	2.46	3.19	144	460
S-band TW (2 m) cavity	1.62	2.31	104	240
S-band TW (2 m) load	1.71	2.22	104	231
S-band TW (3 m) cavity	2.45	3.50	64	224
S-band TW (3 m) load	1.15	1.50	64	96
Total				2001

3.5 Target area design

Figure 3.7 shows a schematic drawing of the target area. The left part of the figure shows the top view and the right part shows the cross sectional view. The service area where the power source (klystron and modulator) is placed, is separated from the accelerator area with 1.5 m concrete shield as same as in the main linac area.

The service area is 3.5 m wide. The power source for the E-driven positron source (L-band and S-band) was designed by Scandinova Co. and presented in KEK on 6. October 2017[59]. Table 3.3 and 3.4 summarize the parameters for L-band and S-band klystron modulator system. The weight of each power source is 3300 kg for L-band and 4500 kg for S-band, respectively. The weight includes klystron, solenoid magnet, oil, etc.

The power sources are designed based on K300 and K400 platform by Scandinova Co. as shown in Fig. 3.5 and 3.6. The system is integrated with solenoid power supply, Ion-pump power supply, RF driver amplifier, cooling water circuit for klystron (collector and body) and solenoid, and all diagnostics and interlocks. The dimensions are 1420 (depth) x1894 (width) x1927 (height) for L-band 50 MW and 1725 (depth) x 2447 (width) x1982 (height) for S-band 80 MW. The size is in mm.

According to Scandinova company[59], 600 mm space is required for the maintenance, because the maintenance is done by exchanging sub-units and klystron and there is no need to transport the whole unit after installation. We reserve the space for the maintenance (0.6 m) and transportation of klystron along the service area tunnel (1.2 m).

The positron target area is isolated from the other area of the accelerator tunnel with 1000 mm borated concrete tunnel. The target activity after 5000 hours operation and 1

EDMS Nr.: D00000001165115 Rev: B Ver: 3 Status: Released - for publication Dat.: 23. May 2018

Table 3.3: Paramters of L-band RF power source (klystron and modulator) designed by Scandinova Co.[59]

Parameter	Value	Unit
RF frequency	1300	MHz
RF peak power	50	MW
RF average power	7.5	kW
Mod. peak power	76	MW
Mod. average power	42	kW
Klystron voltage	271.7	kV
Klystron current	282	A
RF pulse width (top)	0.5	μ s
Pulse repetition rate	300	Hz
Pulse-to-pulse stability	¡20	ppm

Table 3.4: Paramters of S-band RF power source (klystron and modulator) designed by Scandinova Co.[59]

Parameter	Value	Unit
RF frequency	2600	MHz
RF peak power	80	MW
RF average power	12	kW
Mod. peak power	143	MW
Mod. average power	86	kW
Klystron voltage	271.7	kV
Klystron current	282	A
RF pulse width (top)	0.5	μ s
Pulse repetition rate	300	Hz
Pulse-to-pulse stability	¡15	ppm

EDMS Nr.: D00000001165115 Rev: B Ver: 3 Status: Released - for publication Dat.: 23. May 2018

Figure 3.5: Picture of K300 platform for L-band power source.[59]

Figure 3.6: Picture of K400 platform for S-band power source.[59]

hour cooling, is estimated as 7.4×10^{12} Bq for undulator positron generation[56]. The number is similar for E-driven according to T. Takahashi[57] and A. Ushakov[58]. It is 8.2×10^{12} Bqafter 5000 hours operation and 1 hour cooling. The number goes down to $7.4 \times\ 10^{10}$Bq after 2 years cooling. The radiation dose at 400 mm from the target (no shield) is $2.0 \times 10^{5}\mu$Sv/h after 5000 hours operation and 1 hour cooling. This number can be decreased with 750 mm borated concrete shield down to 30μSv/h. Including a safety margin, 1000 mm borated concrete as the shield is assumed to guarantee less than 20μSv/h in the working area. This number can be decreased down to less than 1μSv/h by 2 years cooling.

In this estimation, the radiation activity of the shield is not accounted. In reality, the shield is activated by particles scattered from the target and the Radiological activity from the shield could be dominant. To minimize the radiation dose in the accelerator tunnel, the shield configuration should be studied well, but it is a next issue.

The target is replaced annually, once in year, even the target is operable for more than 2 years, according to the radiation damage of the target material. The target module contains: target, rotor, FC, and vacuum vessel. Due to the high radiation dose in the area after operation, the target module should be replaced remotely without any direct access by human. The first RF module is also replaced remotely, but it is separately. The maintenance for the downstream area of the 2nd RF, can be made manually, when the target and 1st RF are removed, with an appropriate tentative shield.

In the remote handling of the target and 1st RF modules, several connections should be also managed remotely. It is water supply, electricity, and vacuum line (beam line) for the target module, and RF wave guide for the 1st RF module additionally. There is commercially available "one touch joint" for the water line and electricity, but they are not compatible to the high radiation environment. Based on the commercial product, we have to develop the device compatible to the high radiation environment. This is true for the vacuum line connection, e.g. inflatable vacuum seal can be used for the remote control for the vacuum line, but the robustness for the high radiation environment should

EDMS Nr.: D00000001165115 Rev: B Ver: 3 Status: Released - for publication Dat.: 23. May 2018

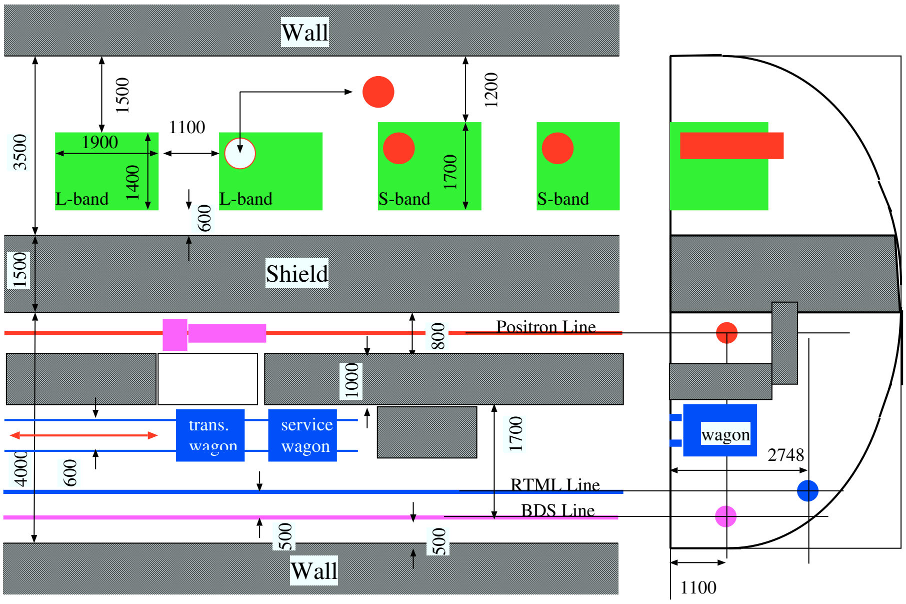

Figure 3.7: A schematic drawing of the target area.

be examined. The remote control for the RF connection to the 1st RF (wage guide) could be the most critical. It is not a simple vacuum connection, because the two surfaces of each joint should be well aligned. Otherwise, we will have troubles, such as discharge, etc.

The target module and 1st RF module are extracted from the beam line by a remote handling system and installed in a cask on the transportation wagon. The cask is made from 70 mm Pb for the radiation shield. The radiation dose should be below 20 μSv/h to transport the wagon. If we assume the dimension of the cask as 800 × 1500 × 1200 inner dimension, the weight is 9 tons. The total weight of the wagon (except the truck weight) including the weight of the target or the 1st RF unit, is less than 10 tons. A narrow gauge train, e.g. 600 mm gauge like a mine train, is suitable to transport the wagon, because a typical maximum load per axis of such train is 9 tons. Two axis wagon is enough to transport the cask. Transport by a train is also desirable from the safety point of view, because any damage to other components during the transport is much decreased.

The wagon is transported from the target area to the target install and storage area as shown in Figure 3.8. The area is in the upstream of the electron driver linac for the positron production where there are only RTML and BDS beam lines and no positron beam line. The used target is stored in the area as packed in the cask. The surface radiation dose at the cask is expected to be 0.1 μSv/h after two years cooling. If one scheduled and one accidental exchanges per one year are assumed, the storage area should keep up to four target units to reserve two years cooling. The used target unit in the cask after the cooling can be transferred to outside of the accelerator tunnel, e.g. the storage area on surface.

EDMS Nr.: D00000001165115 Rev: B Ver: 3 Status: Released - for publication Dat.: 23. May 2018

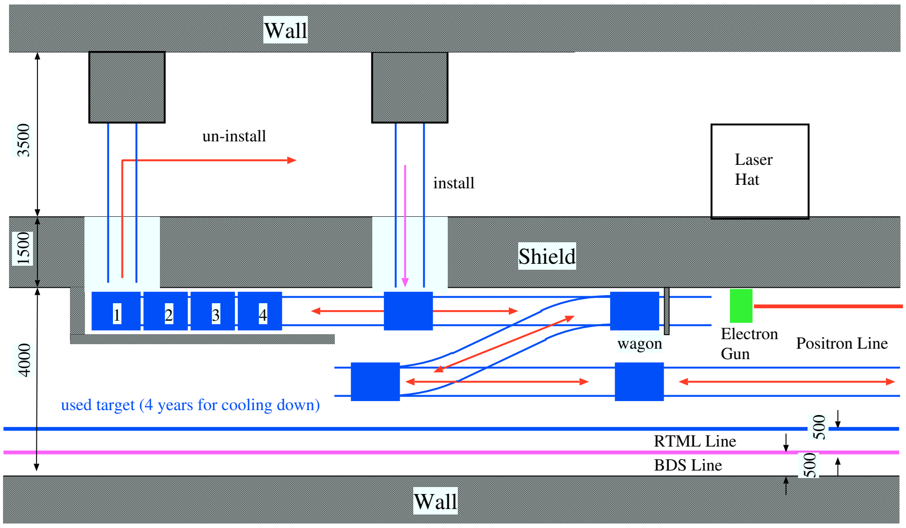

Figure 3.8: Target install and storage area.

3.6 Target for the e-Driven Scheme

3.6.1 Target design

In order to mitigate the heat and stress issues caused by the electromagnetic shower, rotation target is employed in the e-driven positron source. The tangential speed of 5 m/s is required. The size of the target disk is 0.5 m in diameter and rotation speed is 225 rpm.

The disk consists of two parts. One is the outer part ring which is made by tungsten alloy. This part is actually the target of the drive electron beam. The width and thickness of the ring are 20 mm and 16 mm, respectively. The other is the inner part disk which is made by copper. In the disk there are water channels for cooling. The ring and the disk are joined by brazing. There is no water channel in the tungsten ring. The rotation shaft penetrates the vacuum vessel and is connected to the copper disk. The ferrofluid rotation vacuum seal is employed to achieve good vacuum with rotation. Figure 3.9 shows the overview of the rotation target. The central part of the target rotation system which consists of motor, bearing, and the vacuum seal is located upstream of the target disk. There is rather a free space at the downstream of the disk in order to install the flux concentrator near the disk as much as possible.

About the brazing between copper disk and tungsten ring, we have a plan to perform thermal cycle test in the future. If brazing doesn't work, to bolt tungsten pieces to the Cu wheel may be an alternative choice.

The shaft has water channels inside. Cooling water goes into the copper disk trough the shaft then water running inside the disk to remove the heat. Finally the water comes out through the shaft. The shaft is made of copper because the inner part disk is made of copper. With this we can avoid the dissimilar metal junction of water channel in a vacuum.

Figure 3.10 shows the design of the central part of the rotation target. The ferrofluid rotation vacuum seal is located at nearest to the vacuum. Two mechanical bearings are located in the air side of the system and support the weight of the target. The vacuum seal does not support the weight at all. The mother is located between two mechanical

EDMS Nr.: D00000001165115 Rev: B Ver: 3 Status: Released - for publication Dat.: 23. May 2018

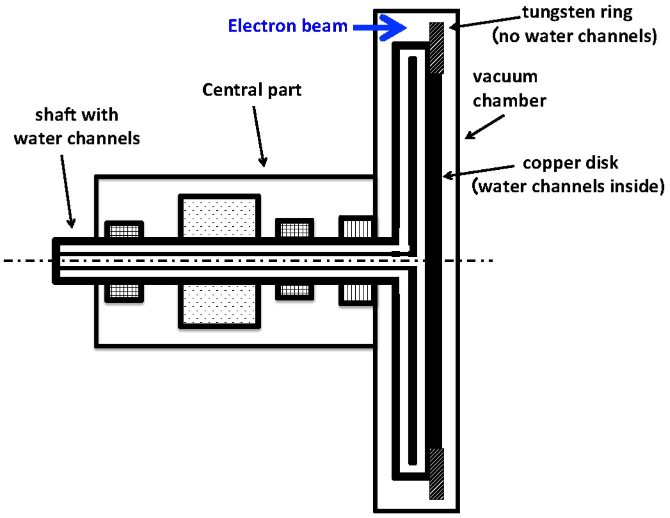

Figure 3.9: Conceptual view of the rotation target. The disk consists of two parts. One is the outer part ring which is made of tungsten alloy. The other is the inner part disk which is made of copper. In the disk there are water channels for cooling. There is no water channel in the tungsten ring. The rotation shaft penetrates the vacuum vessel and is connected to the copper disk. The shaft has water channels inside. The details of the central part are described in Figure 3.10.

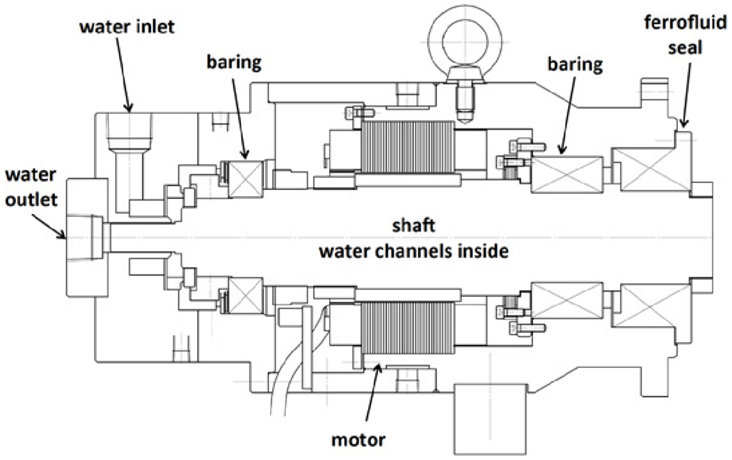

Figure 3.10: The design of the central part. The central part consists of a motor, two bearings, and the ferrofluid vacuum seal.

EDMS Nr.: D00000001165115 Rev: B Ver: 3 Status: Released - for publication Dat.: 23. May 2018

bearings.

The overall design, the design and fabrication of the central part prototype, the heat and stress simulations, and the radiation tests were performed by the close cooperation with Rigaku Corporation.

3.6.2 Heat and stress simulation

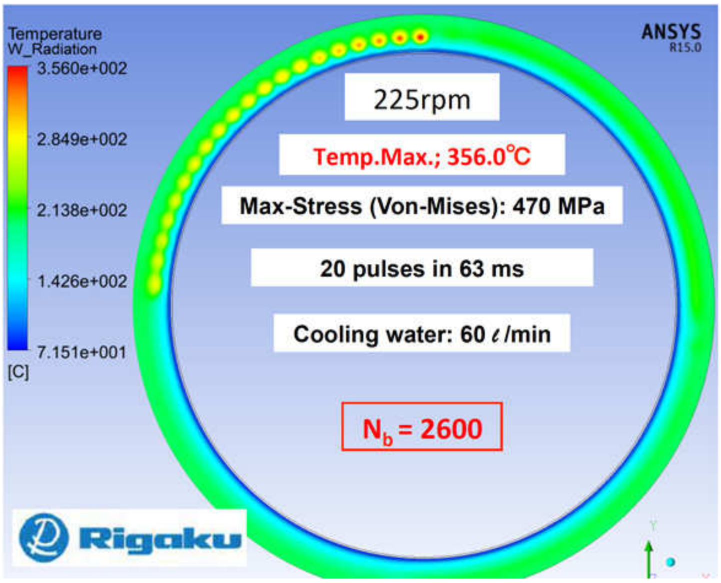

Figure 3.11: The result of the heat and stress simulation.

Figure 3.11 shows the result of the heat and stress simulation. In the simulation, we assumed 5 GeV electron beam, 64 bunches in a mini-train, 2×10^{10} electrons per bunch, about 2600 bunches in macro-pulse in total (20 mini-trains in macro-pulse), and 4 mm spot size of the electron beam on the target (RMS). Since the time duration of the mini-train is about 1 micro sec, we assume all bunches in the same mini-train hit at the same point of the target even the target rotates. Cooling water of 60 liters/min was assumed. This assumption is not exactly the same as the latest design[1] which is optimized for the 1300 bunch operation. The PEDD in the simulation and in the latest design is almost the same. Average heat in the simulation is twice of that in the latest design. Therefore, if we conclude that the target survives in the simulation, we can also get the same conclusion in the latest design. The simulation shows that the temperature of the hottest point is 366 C and maximum stress is 470 MPa. The stress value is very close to the estimated fatigue stress limit of 520 MPa at 500C. In this point of view, the situation is marginal. On the other hand, 470 MPa is very close to the stress of the SLC positron production target, which survived several years before it was broken by repeated stress. If we compare the number of hits per unit length in a year, the number in ILC is[2] 2.1×10^6 pulses/year/mm and that in SLC is 2.1×10^7 pulses/year/mm. The number in ILC is significantly smaller than that in SLC, because ILC target is much larger than

---

[1] In the latest design, 3 GeV electron beam, 32 bunches in a mini-train, 2×10^{10} electrons per bunch, about 1388 bunches in macro-pulse in total (20 mini-trains in macro-pulse), and 2 mm spot size of the electron beam on the target (RMS) are assumed.

[2] In ILC we count a mini-train as a pulse.

SLC target. From the comparison we can conclude that the ILC target disk will survive several years even in the 2600-bunch high-luminosity operation.

3.6.3 Vacuum test of the prototype

The prototype of the central part was built for the vacuum test. This prototype has no disk due to budget limit but it is designed to be compatible with the real target with 500 mm-diameter disk. The bearings and the shaft are designed to be able to support real size target disk which weighs about 70kg. The shaft has two coaxial water channels inside. We ran water in the channel during the test. The shaft is made of copper as same as the design of the real target.

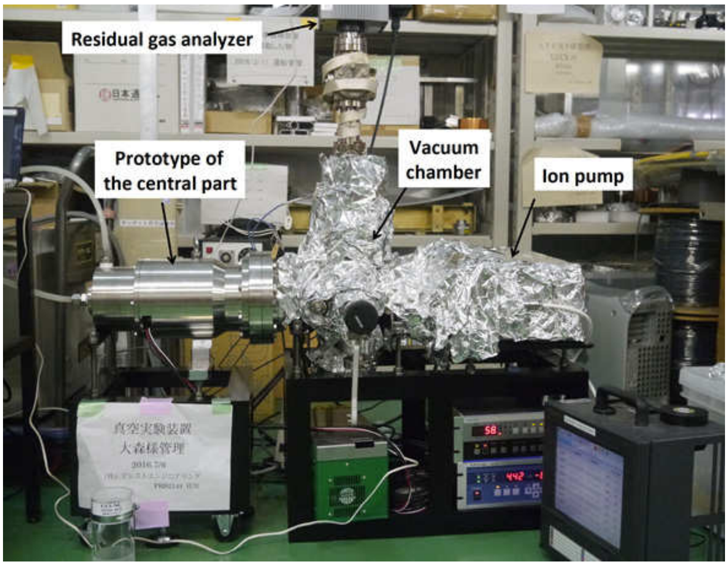

Figure 3.12: The apparatus to test the prototype. It consists of the prototype of the central part, a vacuum chamber, an iron pump of 100 l/min, and a residual gas analyzer with an electron multiplier tube.

Figure 3.12 is a photo of the apparatus to test the prototype. It consists of the prototype of the central part, a vacuum chamber, an iron pump of 100 l/min, and a residual gas analyzer with an electron multiplier tube. A small chiller was used to cool the cooling water.

We have achieved the vacuum level of 5×10^{-7} Pa with 225 rpm rotation. The vacuum level is 5-10 times better than the ILC requirement of 10^{-6} Pa. Furthermore the vacuum was measured at just downstream of the rotation shaft. By assuming 100 l/s pumping speed of the system, the gas desorption rate is estimated as 5×10^{-8} Pa·m^3/s. The calculation shows that we can achieve from 7×10^{-8} to 4×10^{-9} Pa at the first accelerator tube if we assume the same rate (See 3.6.5). Therefore we evaluated that the performance of the rotation seal was basically sufficiently good to use in the ILC positron source. However we still have one concern. As shown in Figure 3.13, the base pressure was about 5×10^{-7} Pa, but we observed sudden jumps of the pressure. The frequency of the jump was once per several hours and the pressure at the peak of the jump was about 2×10^{-5} Pa. The typical duration of the pressure jump was 1-3 minutes. Since the pressure at the first accelerator tube is estimated to be about factor 10 lower than that of

EDMS Nr.: D00000001165115 Rev: B Ver: 3 Status: Released - for publication Dat.: 23. May 2018

at just downstream of the rotation shaft, the jump is maybe acceptable. Nevertheless, in the viewpoint of the long term stable operation of the capture section, we consider means to remove the pressure jumps. The two-stage vacuum seal is now under consideration to overcome the issue.

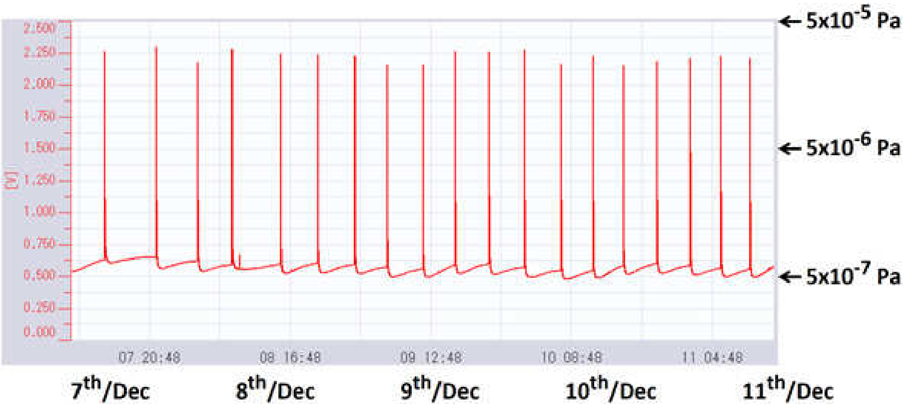

Figure 3.13: The vacuum level measured in the operation of the prototype at 225 rpm rotation speed. The pressure was about 5×10^{-7} Pa basically, however we observed jumps of the pressure in every several hours. The typical height of the jump was 2×10^{-5} Pa and duration was 2-3 minutes.

3.6.4 The irradiation tests

Irradiation test of the ferrofluid

We made systematic test of ferrofluid up to 4.7 MGy. Figure 3.14 is the photo of the test. The 4.7 MGy corresponds to the dose of ILC e-driven positron source at the position of the ferrofluid vacuum seal after three-year-operation with high-luminosity mode (2600 bunches). The ferrofluid did not resolve up to 4.7 MGy but viscosity was increased. Figure 3.15 shows viscosity as a function of dose. We installed 4.7MGy-irradiated-fluid into an off-the-shelf small rotation target and made rotation test up to 600 rpm. The target holded the vacuum in the test. The result shows, in practical point of view, the ferrofluid can be effective up to 4.7 MGy dose and can be used for the ILC positron source.

We are now performing another test up to 4.7 MGy. We irradiated both base oil and ferrofluid. The irradiated samples of various dose levels will be analyzed by using gel permeation chromatography and UV-VIS absorption spectroscopy, in order to determine the change of chemical composition of the oil.

In addition, we will install irradiated ferrofluid into the prototype rotation target and check the performance in the long term test.

Irradiation test of a whole target system.

The rotation target system consists of several materials, such as various metals, permanent magnets, insulators, and so on. Such materials should be tested by irradiation. For the test we irradiated a off-the-shelf small rotation target. Figure 3.16 is the photo of the test. Since the design of the ILC rotation target and that of the off-the-shelf small

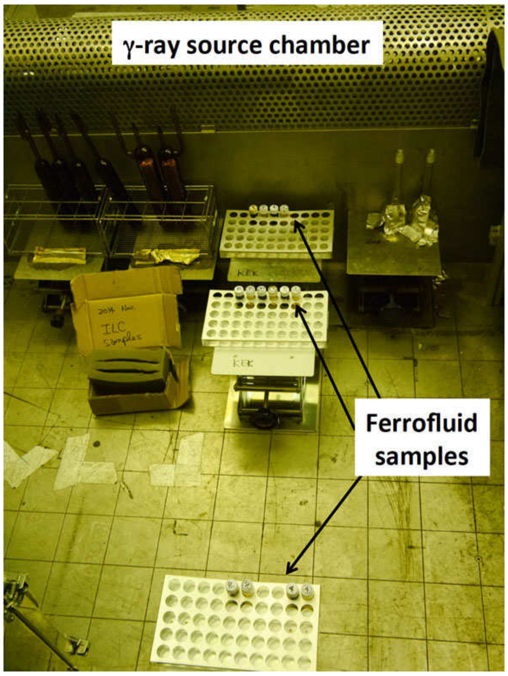

Figure 3.14: The ferrofluid samples in the gamma-ray irradiation chamber of Takasaki Advanced Radiation Research Institute.

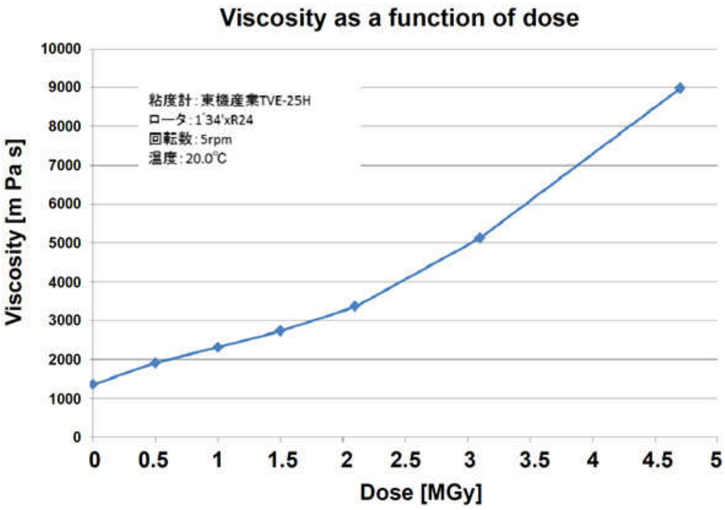

Figure 3.15: The viscosity of ferrofluid as a function of dose.

rotation target are especially the same in viewpoints of materials, the irradiation on the small target represented the real situation. The dose on the small target was 0.6 MGy at the position of the motor, which corresponds to the dose at the motor of the ILC target after one-year-operation in the high-luminosity mode. After the irradiation, we operated the target. The target sustained the vacuum and rotated without problems. Therefore we concluded that, not only the ferrofluid, all materials of the ILC target can survive ILC environment at least 1 year.

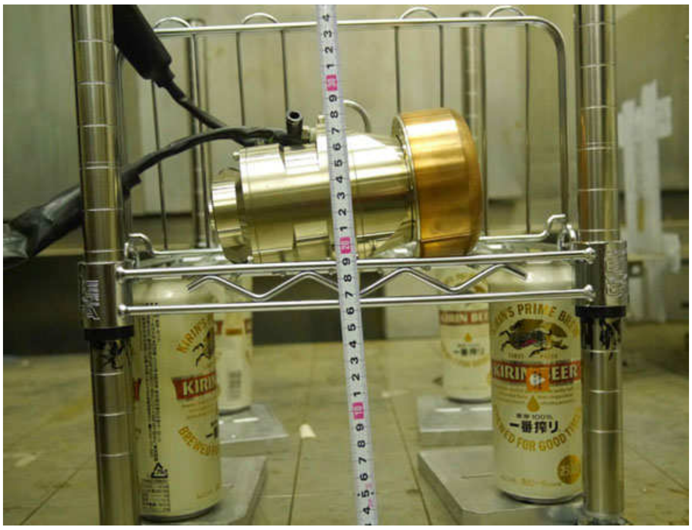

Figure 3.16: A off-the-shelf small rotation target placed in the gamma-ray irradiation chamber for the test.

3.6.5 Estimation of the vacuum level at the accelerator section.

The gas rate from the ferrouid seal is 5×10^{-8} Pa m^3/s. This number is estimated from the vacuum pressure measured in the seal test, 5.0×10^{-7} Pa by assuming 100 l/s pumping speed. The gas flow of the ILC positron target system is modeled as shown in Figure 3.17, where the system is pumped by a large pump with 1000 l/s in the target and a medium pump with 400 l/s at the downstream of the accelerator tube. The clearance between the target surface and the seal unit and flux concentrator surface is 5 mm. The space between the seal unit and FC is filled with a heavy material for radiation shielding for the seal unit against the radiation from the target and FC. Other space than the shield is available for pumping.

The conductance to the nearest pump is estimated to be 306 l/s based on the open area. The conductance to FC is estimated for the narrow channel between the target and the shield or FC surface, a fan shape channel with 5mm thickness. The conductance from the seal to the accelerator tube is 11.6 l/s. The accelerator tube has also a conductance with 23.7 l/s which is estimated as 60 mm diameter tube with 1.1 m length. With this model, the vacuum pressure near the seal is estimated to be 2×10^{-7} Pa. The pressure in the target chamber (an open space for pumping) is 5×10^{-8} Pa. The vacuum pressure in the accelerator is from 7×10^{-8} to 4×10^{-9} Pa. The highest one is that at the entrance, and the lowest one is that at the exit.

3.7 Flux concentrator for the e-Driven Scheme

Flux concentrator is a well and long-time known device for generating high longitudinal magnetic field. Making a conical profile of inside FC cavity for example, a magnetic field

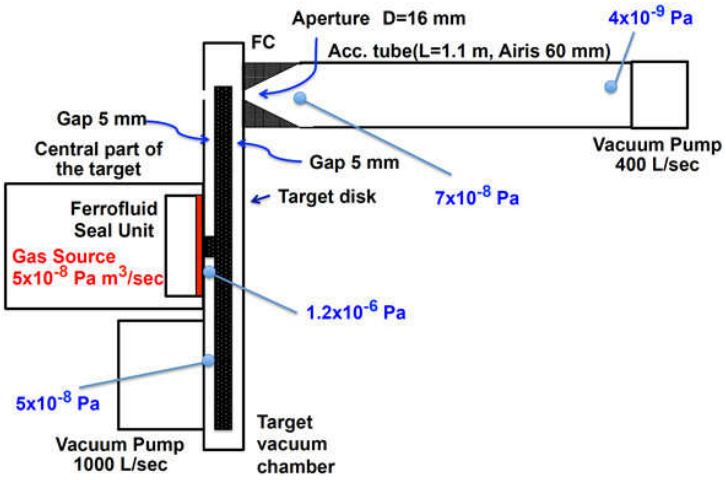

Figure 3.17: The model assumed in the calculation of the gas flow of the ILC positron target system.

also should vary along longitudinal axis from a peak field value. Well-known classical FC consists of two parts: firstly a relatively big and massive FC body fabricated from well-conducting metal and, secondly, winding placed around the FC body. The FC body has a transverse slit from inside cavity to FC a side. The typical width of this slit is about 0.2-0.4 mm and is determined by technical reasons. In practice the annealed copper is used for FC fabrication. The design of a classical FC is not free from technical disadvantages. The open slit makes the FC body insufficiently strong mechanically against the magnetic field force. The second disadvantage is a primary winding holding around FC body and a primary winding insulation. The classical FC is not optimized well from the Ohmic losses point of view. It becomes clear, taking into consideration a current path length of classical FC winding and eddy current path length generated around of FC body. Thus, the classical FC is not well suited to install to a positron source as a matching devise. The single-turn version of the magnet is distinguished by the simplicity of the design of conical part, which is connected to the cylindrical cavity with the help of a flat slit, the primary winding of the pulsed transformer being located in the cylindrical cavity. The computer model of single-turn modification of FC without target is shown in Figure 3.18. Specific for such a load made as a cone is a very low inductance value. Therefore, this low-impedance load required a minimum distance before the pulsed transformer, which is easily achievable in this design and makes its main merit. Mechanical properties of a single-turn version of the magnet obviously are better, because a magnet body is fabricated from a solid piece copper without a slit. A winding holder design also should be simple from technical design of view due to a well centering of one inside of a conical cavity. The magnetic force unbalance along the winding turns is minimized. Radial component of magnetic field force is significantly reduced, because the winding is placed inside of a practically geometry symmetrical cylindrical cavity. A special grooving for the positron production target suppresses a transverse component of magnetic field on the beam line between the target and front face of FC. Main geometrical parameters of single-turn FC are presented in the Table 3.5.

The temperature rise at the tip of the nose by a single pulse ($\sim 1\mu$s) is only a few degrees. Accumulated temperature rise by 20 pulses in 63 ms is expected to be less than 20 times due to thermal diffusion. However, for estimating the stationary temperature

EDMS Nr.: D00000001165115 Rev: B Ver: 3 Status: Released - for publication Dat.: 23. May 2018

cycle the design of the water-cooling system is necessary, but it is yet to be done.

Table 3.5: Main parameters of Single-turn FC.

Shape of FC body	Elliptical cylinder
FC Peak field	5 Tesla
FC size	120×180 mm
Total FC length	170 mm
Conical cavity length	100 mm
Front aperture diameter	16 mm
Rear aperture diameter	64 mm
Cylindrical hole diameter	70 mm
Number of winding turns	16
Turns size	9.6×12 mm
Ohmic loss	14 kW

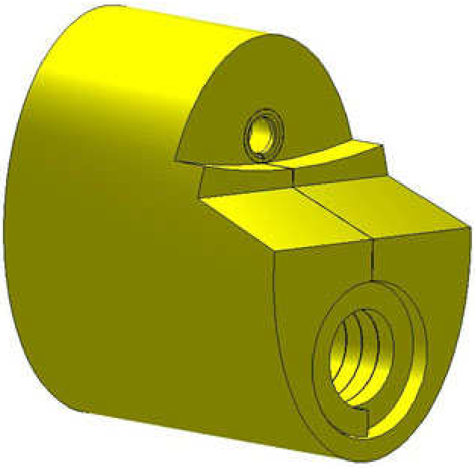

Figure 3.18: Computer model of single-turn modification of FC

EDMS Nr.: D00000001165115 Rev: B Ver: 3 Status: Released - for publication Dat.: 23. May 2018

Chapter 4

CFS Issues

4.1 CFS Issues Related to the Positron Source

There are many CFS issues on the positron source. Notable ones are:

(a) Radiation shield of the target region. A special layout of the target region is necessary, in particular from the target to the capture section (some 10m long).

(b) Target replacement scenario. The life of the target system is limited. It is hard to estimate the life, but one year, for example, is considered to be acceptable. Replacement must be done by a robotic system.

(c) Tunnel crosssection near the target region and the booster linac region.

(d) Logitudinal layout of the tunnel

(e) Housing of the photon dump

Most of these issues are not yet conclusive in spite of variuos studies in our working group. Quite fortunately, there is no essential difference between the two schemes so that these are not critical in the choice of the schemes. Much more serious studies will be done after the project approval.

4.2 Radiation shield of the target region

The region near the target must be enclosed in a specil shield. The basic information should come from the simulation of the radiation dose of this region.

The first step is the modeling of the region for simulation. Figure 4.1 shows an example for the e-driven system[60]. (The radiation dose for the undulator scheme is similar but slightly lower so that studies for e-driven system suffice.)

What must be estimated are:

- Radiation (photon/neutron) distribution and dose during the beam operation
- Accumulated dose in some long-period operation (say, 500 hours)
- Production rate of long-life nuclei such as tritium
- Cooling process after operation stop

EDMS Nr.: D00000001165115 Rev: B Ver: 3 Status: Released - for publication Dat.: 23. May 2018

Figure 4.2 shows a simulation results based on the above model. Obviously, this is only the start of the study.

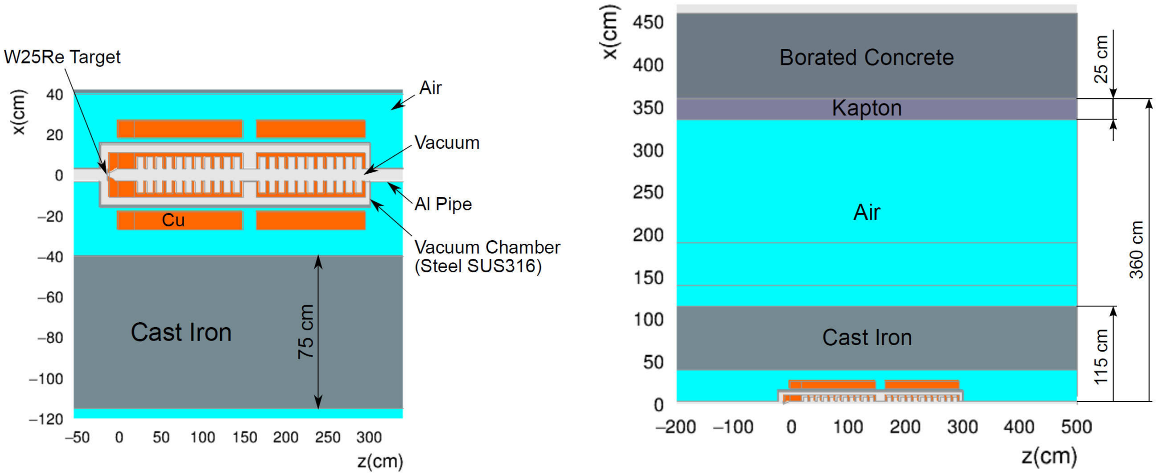

Figure 4.1: A model of the target region for the e-driven scheme. The positron source is placed in parallel with the electron BDS line and is close to the central wall separating the accelerator and service tunnels. The figure on the left shows the positron capture region and the iron shield on the central wall side. The figure on the right shows the region from the capture section (bottom) to the tunnel wall (top) beyond the BDS line (modelled by "air").

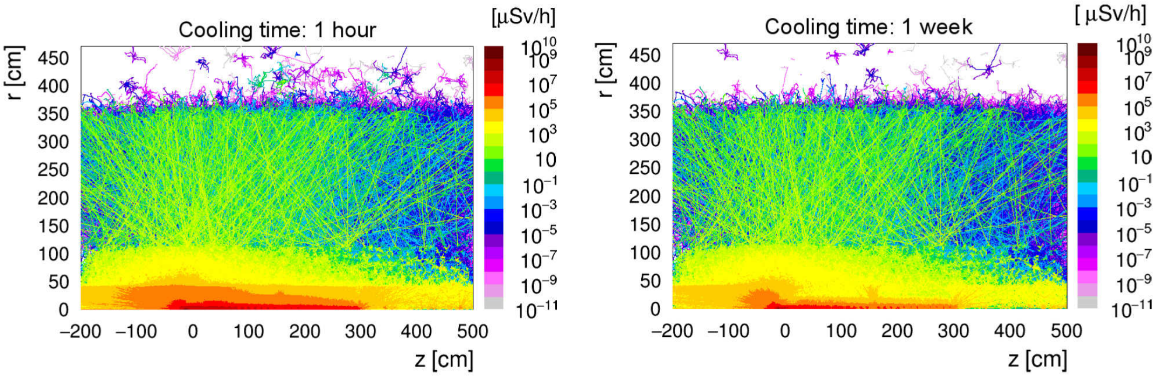

Figure 4.2: An example of the residual dose after 5000 hours of operation and the cooling period 1 hour (left) and 1 week (right).

4.3 Target replacement scenario

The life of the target (and the surroundings) is expected to be quite short compared with the operation time of a given center-of-mass energy. We have to prepare for the target replacement on the order of a year. To design the replacement scenario we have first to give answers to several questions:

EDMS Nr.: D00000001165115 Rev: B Ver: 3 Status: Released - for publication Dat.: 23. May 2018

- How big is the part to be replaced? At present our general consensus is that the target wheel with the rotation system, FC or QWT, the first few cavities (a few meters), and the surrounding solenoid should be replaced.

- Can this part be taken out from the tunnel immediately after its life? Presently, our majority think the radiation level is too high. About 2 years of cooling time is needed. Thus, the used part must be stored in the tunnel for a while. It must eventually be transported to the surface. The path to the surface must be taken into account.

- Where should it be stored? TDR describes a replacement scenario in which the used targets are stored in an upper floor room in the tunnel, but this is not realistic since it requires a large crane. We have to prepare a space to store several sets of the used part. Figure 3.8 shows an example of the storage area for the e-driven system. It occupies some space in the accelerator tunnel. Figure 4.3 shows another example[61], where the working and used targets are housed in a common room separated from the accelerator and service tunnels.

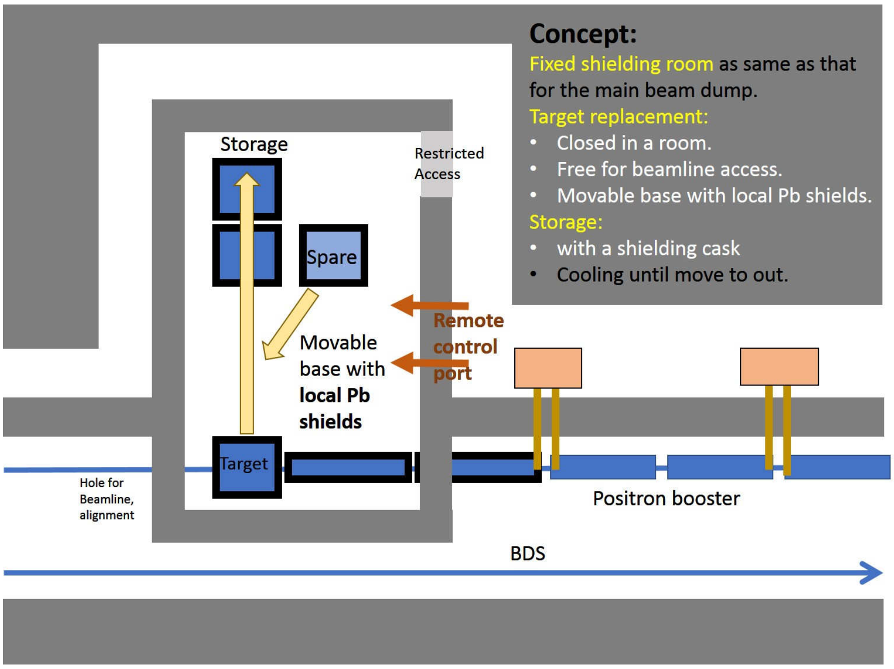

Figure 4.3: An example of the target replacement scenario with a specially shielded room containing the working and used target together.

We expect that there is no significant difference in this respect between the two schemes. More serious studies are obviously needed and will be done after the project approval.

4.4 Longitudinal Layout

The major difference in CFS between the two schemes is the longitudinal layout.

EDMS Nr.: D00000001165115 Rev: B Ver: 3 Status: Released - for publication Dat.: 23. May 2018

Total length of the entire facility is longer for the undulator scheme due to the global timing constraint and the existence of the undulator section. This will cause a difference in the location of the access tunnels. In this respect an early decision is desired to start the CFS design of the tunnel.

Obviously, there must be a space for the undulators for the undulator scheme. The total length of the undulator section is about 1km, including the undulators and the dogleg of the electron beam in parallel with the photon drift line. In the TDR design the length of the section from the IP to the end of the electron main linac is $L_1 = 3489$ m, whereas that from the IP to the end of the positron main linac is $L_2 = 2361$ m. Through these regions the tunnel is laser-straight. (Note that there are soft vertical bends, fraction of milli-radian, at the ends of the main linacs.)

This means that in the TDR design the IP is not at the center of the laser-straight region. Hence, either the orbit at the IP is inclined by $(L_1 - L_2)/(2R) \sim 0.9$mm per 10m ($R =$ earth's radius) if the electron and positron sides are on the same geoid level, or the elevation of the electron side is higher ($L_2(L_1 - L_2)/R \sim 40$ cm) if the tunnel is flat at the IP. On the other hand, in the case of the e-driven system, the laser-straight setion is symmetric (2×2361m).

Thus, the following four cases must be considered in this respect:

- Undulator case
- e-Driven case
- Start with e-driven and later it is replaced by the undulator system.
- Start with e-driven and later the undulator system is added.

However, it turned out that, for the undulator scheme, the undulator section (itself laser-straight, of course) can be installed on the curved floor following the geoid level, by using two vertical bends before and after the undulators.

Figure 4.4 shows the possible vertical layout in the case where e-driven system is initially built and is replaced by undulator system later. In this case the photon dump for the undulator system will be placed up to ∼1 m above the BDS beamline level, if it is located at 1-2 kms from the target as described in Sec.2.6,

Thus, in all the cases above, the laser-straight setion can be symmetric (2×2361m).

Thus, the laser-straight problem would not cause a difference between the two schemes.

EDMS Nr.: D00000001165115 Rev: B Ver: 3 Status: Released - for publication Dat.: 23. May 2018

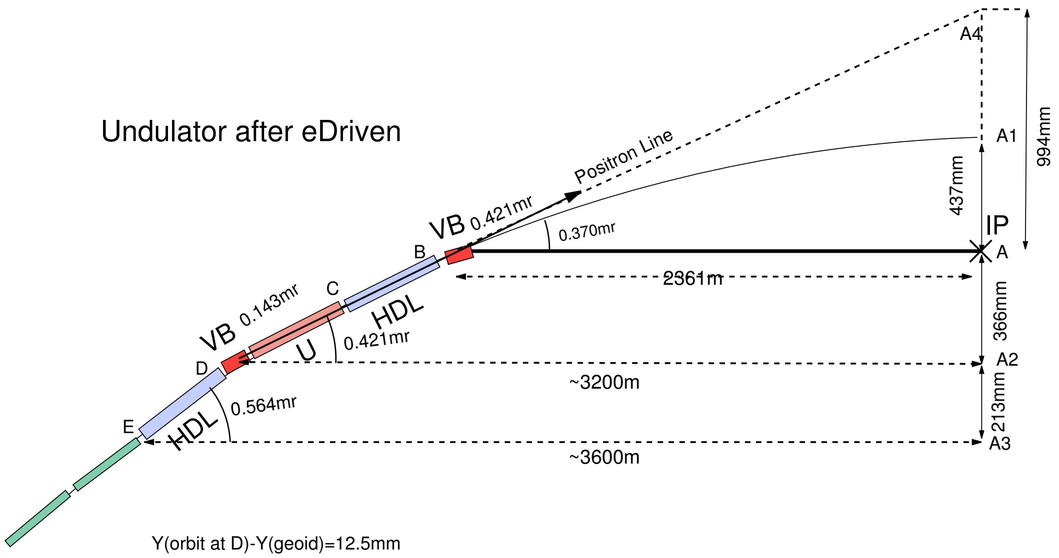

Figure 4.4: Vertical layout from the positron source region to the IP in the case the undulator scheme replaces the e-driven scheme later. VB: vertical bend, HDL: horizontal dogleg, U: undulator section. If the photon dump is placed at ~2km from the target (the point A_4), it will be about 1m above the BDS line (~1.5 m off, horizontally).

Chapter 5

Cost Comparison

Results of the ost comparison between the undulator and e-driven scheme was reported in LCWS2017 at Strasbourg. It is repeated here for completeness. See the reference for more details.

5.1 Cost of e-Driven System

TDR does not describe about the cost (‘value’) of the e-driven positron production system. Japanese members made the first estimation of the cost and it was reviewed in a domestic meeting of a comittee consisting of non-ILC, Japanese accelerator scientists.

The estimation was based on the following parameters

Number of bunches pulse	1312
Pulse repetition frequency	5 Hz
Time to fill the damping ring	63 ms
Time for damping in the damping ring	137 ms
Positron bunch charge (margin factor 1.5)	4.8 nC

The resulting cost numbers are summarized in Table 5.1. Some components such as beam dumps (at the drive linac end, after $e^+e^-\gamma$ separation, after acceleration to 5 GeV) are not included but they are small.

Table 5.1: Basic Cost of Accelerator of e-Driven Positron System (in units of OkuYen $= 10^8$ Yen $\approx$ 1M\$)

Electron drive linac (incl. RF gun and the matching section)	58.58
Target system (target, flux concentrator, solenoid, remote handling)	16.50
L-band capture linac (L-band SW)	32.80
Booster linac (L-band TW, S-band TW)	158.84
Energy compressor (L-band SW)	6.27
Others	5.68
Accelerator sum	272.2
CFS	44.
Total sum	316.

5.2 Cost of Undulator System

TDR quotes 228 MILCU as the value of accelerator components and 72MILCU for the CFS for the undulator positron source. However, these numbers cannot be compared directly with the cost of e-driven system given above because

- There are several design changes since TDR as described in Sec.2.1.
- For the CFS we evaluated only the cost difference between Undulator and e-Driven schemes by counting the addition and elimination.
- For the purpose of comparison with the e-driven system, numbers of items which are included in other area systems have to be included in the cost of the undulator scheme..

There have been following changes since TDR:

- The undulator length (sum of effective length of undulators) has been increased from 147 m in TDR to 231 m for sufficient positron production $E_e = 125$ GeV. (Note that TDR adopted 10Hz operation with 147m undulators.)
- The beam dump of spent electrons after photon production is needed for 10Hz operation. This will not needed in the 250 GeV machine.
- The auxiliary positron source will not be constructed because it is considered not to help much in the commissioning stage perhaps.

The items that are included in other area systems but that must be included in the positron system for the purpose of comparison are:

- The electron loses 3 GeV in the undulator. This must be compensated for in the electron main linac (this is included in the value of the main linac in TDR). The cost of this additional acceleration should be included in the positron system cost. Also, the increase of the corresponding RTML beam line cost should be added, though small.
- After the undulator the electron beam is separated from the photon beam by a dogleg. The cost of dogleg is included in BDS in TDR, but should be moved to positron system. (The actual dogleg which has been re-designed is much shorter for E_e=125GeV because photon emission angle is larger as described in Sec.2.1. This cost difference is not counted for, here.)

The comparison was made by converting the undulator system cost from ILCU (ILC unit) to Japanese Yen, rather than the other way. We used the rule of conversion which was adopted when we explained the TDR value to the Japanese government (MEXT). The resulting cost is shown in Table 5.2.

5.3 Cost Comparison

As presented in the Table 5.1 and Table 5.2 there is no significant cost difference between the two schemes. However, the actual cost of the undulator system depends of the center-of-mass energy because the constraint coming from the global timing condition

Table 5.2: Basic Cost of Undulator Positron System (OkuYen = 10^8 Yen)

	Accelerator	CFS
TDR	227.5	67.
Longer undulator	13.0	0
3GeV compensation	27.	7.3
Dogleg	21.	0
Beam dump for 10Hz	-7.7	0
Auxiliary positron source	-5.9	0
Sum	273.9	74.3

must be satisfied. The additional cost of the empty tunnel for the undulator system due to the timing constraint is about 26 OkuYen and 46 OkuYen for the average accelerating gradient 31.5MV/m (TDR) and 35MV/m (after R&D), respectively.

There is also a complication coming from the upgrade scenario in the case when the project starts with the e-driven system and replacement is done in later time, but this will not be discussed here because there can be different scenarios of upgrade of energy and luminosity.

Thus, in conclusion, the cost difference between the two schemes is not significant, but amounts to several tens of OkuYen (~MILCU) depending on the center-of-mass energy and adopted accelerating gradient.

5.4 Power Consumption

The power consumption of the two schemes has also been compared. The consumption for the undulator scheme is 9.3 MW (TDR vol.3 part II, p.187) plus about 0.6 MW for the compensation of the electron energy loss 3 GeV in the undulator.

The consumption of the e-driven scheme is estimated to be 14 MW, including the power for the two linacs, solenoid (but not including the target and FC, which are minor).

Thus, the difference of the power consumption between the two schemes is only 4 MW, about 3% of the total power consumption of ILC 250GeV.

EDMS Nr.: D00000001165115 Rev: B Ver: 3 Status: Released - for publication Dat.: 23. May 2018

Chapter 6

Summary

The present report have described the present status and scope of the two schemes of positron production, putting emphasis on the contraversy and/or urgent issues.

The technology status of the undulator and e-driven schemes were summarized in the AWLC2017 at SLAC[63]. It was a result of the discussion within the positron working group. The present status is essentially the same as at AWLC2017. Here, the summary table is reproduced (Table 6.1) with a few updates. (See the reference for the details of the individual components.)

Table 6.1: Summary of the technology status of the two schemes

	Undulator Scheme		e-Driven Scheme	
Target	Further consideration on wheel design, cooling calculation, mechanical performance (magnetic bearing), and Ti-Cu contact needed. Prototype shoud be built.	C	Further test of vacuum seal needed. W-Cu contact must be studied.	B
Matching device	FC has the problems of time-dependent field and PEDD.	D	Improvement from superKEKB and BINP. Design of cooling needed.	B
	QWT: yield marginal. Hardware design still required.	B		
Capture cavity	TDR design almost sufficient	A	Further consideration on thermal deformation and cavity cooling design needed	B
Beam dump	Photon dump still requires detailed design.	C	Beam dump is not an issue but radiation shielding must be studied instead.	B

In this table the status of each component is labeled in five levels:

A Complete model or some prototype exists. Can be finalized if tried.

EDMS Nr.: D00000001165115 Rev: B Ver: 3 Status: Released - for publication Dat.: 23. May 2018

B Basic partial tests done or known to work. No whole prototype.

C Calculation study only. But no show stopper seen yet.

D Break through needed.

E There is a fatal problem.

A few comments on this table:

- Here, driver beam, booster linac and yield simulation are omitted. These are more or less in the state B or better for both schemes.
- The flux concentrator for the undulator scheme is assigned D. However, as explained in Sec.2.1, the positron yield with QWT is nearly enough, though marginal. Thus, we can eliminate the row for FC of undulator scheme.

Note, however, this table does not mean that every member agrees on the status evaluation of individual items. Some of them suggest to assign severer scores for some items. Re-evaluation of the table is inevitable in the near future by the time to down-select the scheme. But it is more important to make a complete "ToDoList" for each item as stated above.
As shown in the previous section

- The cost of the accelerator components for the two schemes are almost the same.
- The CFS cost of the undulator scheme is higher due to the tunnel longer by ∼2 km.
- The power consumption of the e-driven scheme is larger by ∼4 MW.

But these are not a decisive factor in the choice.

As the table shows, the technology for neither scheme is ready now. Among the two the e-driven scheme seems to be closer to realization, judging from the present status of prototype development. On the otherhand, the baseline scheme, *i.e.*, the undulator scheme, if feasible, has an advantage of the positron polarization. Therefore, the primary question for the choice of the scheme is

- Is the undulator scheme feasible?
- If so, can the feasibility be firmly verified by the time of design finalization?

We do not know clearly when is the deadline for the decision, but it is not too far, within a couple of years. In this respect of the project schedule we need a guidance from TCMB or LCC.

The working group hope that this report gives useful information for the decision in the near future.

EDMS Nr.: D00000001165115 Rev: B Ver: 3 Status: Released - for publication Dat.: 23. May 2018

Bibliography

[1] ILC Technical Design Report, Vol.3.II Accelerator Baseline Design, also vol.3.I Accelerator R&D,
https://www.linearcollider.org/ILC/Publications/Technical-Design-Report

[2] K. Fujii *et al.*, "The role of positron polarization for the initial 250 GeV stage of the International Linear Collider," arXiv:1801.02840 [hep-ph].

[3] T. Okugi, "Compact dog-leg design for 125 GeV electron beam",
https://agenda.linearcollider.org/event/7573/contributions/38619/attachments-/31296/47039/PosiPol_okugi_20170316.pdf

[4] DJ. Scott, Phys. Rev. Lett. 107 (2011) 174803.

[5] T. Okugi, KEK domestic meeting on Mar. 15, 2018,
http://atf.kek.jp/twiki/pub/ILCpositron/WeeklyMeetingKEK/PosiPol_okugi_20180315.pdf

[6] T. Behnke *et al.*, "The International Linear Collider Technical Design Report - Volume 1: Executive Summary," arXiv:1306.6327 [physics.acc-ph];
C. Adolphsen *et al.*, "The International Linear Collider Technical Design Report - Volume 3.I: Accelerator R&D in the Technical Design Phase," arXiv:1306.6353 [physics.acc-ph];
C. Adolphsen *et al.*, "The International Linear Collider Technical Design Report - Volume 3.II: Accelerator Baseline Design," arXiv:1306.6328 [physics.acc-ph].

[7] A. Ushakov, Talk given at POSIPOL, August 2016, Orsay, France.
https://indico.lal.in2p3.fr/event/3288/contributions/8120/attachments/7640/9004/-Ushakov-POSIPOL2016.pdf

[8] A. Ushakov, G. Moortgat-Pick, and S. Riemann,
arXiv:1801.08465 [physics.acc-ph], Jan 2018.

[9] A. Ushakov *et al.*, "Simulations of the ILC positron source at low energies", 4^{th} International Particle Accelerator Conference (IPAC13), Shanghai, China, 12-17 May 2013, pp. 1562-1564, TUPME003;
A. Ushakov, Talk given at the ILC Staging Mini-Workshop, April 5-7, 2017, KEK, Japan.

[10] K.C. Mills, 2002, Recommended Values of Thermophysical Properties For Selected Commercial Alloys, 1st edition; eBook ISBN: 9781845690144; Woodhead Publishing, 22nd April 2002, p.217.

[11] S. Riemann, F. Dietrich, G. Moortgat-Pick, P. Sievers and A. Ushakov, arXiv:1801.10565 [physics.acc-ph]; https://arxiv.org/pdf/1801.10565.pdf.

[12] ATI manufacturer, product documents: https://www.atimetals.com/Products/Documents/datasheets/titanium/alloyed/ati_6-4_tds_en_v1.pdf

[13] P. Marmy *et al.*; "The tensile and fatigue behavior of thetitanium alloys Ti6Al4V and Ti5Al2.4Sn before and after irradiation with protons to doses up to 0.3 dpa"; ITER TASK BL 14.2: Titanium Alloys Irradiation Testing; https://infoscience.epfl.ch/record/121248/files/lrp_695_01_hq;
P. Marmy and T. Leguey, "Impact of irradiation on the tensile and fatigue properties of two titanium alloys",Journal of Nuclear Materials 296 (2001) 155-164;
R.O. Ritchie *et al.*; "High-cycle fatigue of Ti-6Al-4V", 1999 Blackwell Science Ltd. Fatigue Fract Engng Mater Struct 22, 621-631;
https://onlinelibrary.wiley.com/doi/epdf/10.1046/j.1460-2695.1999.00194.x.

[14] MatWeb Titanium Alloy Property Data; http://www.matweb.com/reference/titanium.aspx

[15] Valbruna Ti6Al4V, https://www.valbruna.de/de/werkstoff/3.7164-3.7165.html

[16] A. Ushakov *et al.*, Talk given at POSIPOL 2014, Ichinoseki, August 2014.

[17] M. Breidenbach *et al.*, "A Positron Target Concept for the ILC", 38th International Conference on High Energy Physics (ICHEP), Chicago, August 2016.

[18] A. Fassò *et al.*, "FLUKA: a multi-particle transport code", CERN-2005-10 (2005), INFN/TC-05/11, SLAC-R-773.

[19] ANSYS, http://www.ansys.com.

[20] F. Staufenbiel *et al.*, "Heat Load, Stress and Reaction Force Studies of a Polarized Positron Production Target for the ILC", 5th International Particle Accelerator Conference (IPAC 2014); June 2014, Dresden, Gemany; TUPME001.

[21] P. Heil et al., "High Energy Density Irradiation With MAMI LINAC", 8th International Particle Accelerator Conference (IPAC 2017), 14-19 May 2017; Copenhagen, Denmark. TUPAB003.

[22] A. Ushakov *et al.*, "Material Tests for the ILC Positron Source", 8th International Particle Accelerator Conference (IPAC 2017), 14-19 May 2017; Copenhagen, Denmark. TUPAB002.

[23] A. Ushakov et al., talk given at ECFA-LC 2016, May 30 - June 5, Santander, Spain; https://agenda.linearcollider.org/event/7014/contributions/34633/attachments/-29960/44797/Ushakov-PhotonDump-ECFALC16.pdf

[24] Advanced Material Technology (AMT), High temperature Titanium alloys, Ti-SF61.

[25] Dubbel, "Taschenbuch für den Maschinenbau". Eds. K.-H. Grote, J. Feldhusen, 21. Auflage, Springer.

EDMS Nr.: D00000001165115 Rev: B Ver: 3 Status: Released - for publication Dat.: 23. May 2018

[26] K. Yokoya, Talk given at Asien Linear Collider Workshop (AWLC), 20-24 April 2015, Tsukuba, Japan.

[27] I. Bailey *et al.*,

"Eddy Current Studies From the Undulator-based Positron Source Target Wheel Prototype", Conf. Proc. C **100523** (2010) THPEC033.

[28] Chromalox, Advanced Thermal Technologies,
https://www.chromalox.com/en/catalog/component-technologies/cartridge-heaters;
WATLOW, http://www.watlow.com/products/heaters/cartridge-insertion-heaters

[29] P. Sievers, Talk given at POSIPOL 2013, Argonne, France.

[30] S. Riemann, LCWS2017, Strasbourg, 23-27 Oct. 2017.

[31] P. Sievers, to be published.

[32] P. Sievers, Talk given at POSIPOL 2017 at Budker INP-Novosibirsk, 18-21 Sept. 2017.

[33] P. Sievers, Talk given at a Work shop in 2017 in Itako-Japan.

http://home.hiroshima-u.ac.jp/ mkuriki/2017Itako/

[34] M. Maslov, M. Schmitz and V. Sychev, Layout considerations on the 25 GeV /

300 kW beam dump of the XFEL project", August 2006, 72 p., DESY, TESLAFEL 2006-05.

[35] ILC Technical Design Report volume3 part II 5.5.7 "Electron & photon beam dumpsh

[36] P Sievers, A. Ushakov, Presented at the ECFA LC 2016- Santander, 30 May- 4. June, 2016.

[37] Y. Morikawa, "A Photon Dump Study for ILC Undulator Positron Sourceh Presented at the LCWS2017- Strasbourg, 23-27 Oct, 2017.
https://agenda.linearcollider.org/event/7645/contributions/40016/attachments/-32407/49219/LCWS2017-ilcphotondump.pdf

[38] T. Omori, et al., NIMA(672)(2012)52.

[39] B. List, Harmonic Number for the ILC Damping Rings, ILC EDMS ID:960865(2011).

[40] ILC Technical Design Report (2013).

[41] Y. Seimiya et al, "Positron capture simulation for the ILC electron-driven positron source",Prog. Theor. Exp. Phys. (2015) 103G01.

[42] M. Kuriki et al., "The latest results of the start to end simulation of E-driven ILC positron source", AWLC2017, SLAC (2017).

[43] T. Okugi, A talk in a domestic meeting in Japan, Mar.8.2018. http://atf.kek.jp/twiki/pub/ILCpositron/WeeklyMeetingKEK/PosiPol_okugi_20180308.pdf (in Japanese)

[44] JPS annual meeting, at Tokyo University for Science, 2018.

[45] T. Kamitani and R. Louis, "Positron production at CLIC", CLIC-note-465, 2000.

[46] ATF design report, KEK Internal 95-4, 1995.

[47] J. Urakawa, "Beamloading Compensation Test for 300 Hz Linac", Posipol 2014, Ichinoseki, Japan(2014).

[48] M. Kuriki et al., "A design study of ILC positron source based on electron driven scheme", Private Note (2016).

[49] T. Omori, "Target R&D Status of E-driven ILC Positron Source", *LCWS2017*, 2017.

[50] J.W. Wang, C. Adolphsen, V. Bharadwaj, G. Bowden, E. Jongewaard, Z. Li, R. Miller, J. C. Sheppard, SLAC-PUB-12412(2007).

[51] Masao KURIKI, "Beam-loading compensation for the multi-bunch and multi-pulse acceleration", Private Note (2015).

[52] Masao KURIKI, "A simulation study for the positron capture linac of the e-driven ILC Positron Source with L-band standing wave accelerator"Private Note (2015).

[53] S. Matsumoto, et al.,"L-band Accelerator System in Injector Linac for SuperKEKB".

[54] S. Matsumoto, et al., THPR1047, *Proc. of IPAC2014*(2014).

[55] H. Matsumoto, "10 MeV Linac For OIST-BNCT", OIST seminar (2015)

[56] Jia Xuejun, "Remote Handling of ILC Target", *KILC 12* , April 24, 2012, Daegu, Korea.

[57] T. Takahashi, "Energy deposition around the target of the E-driven e+ source", AWLC2017.

[58] A. Ushakov, et al., "Shielding in Target Area of Conventional Positron Source", Itako Linear Collider Workshop, at Itako, Chiba, Japan(2017)

[59] P. Akersten (Scandinova), "Solid-state modulator design adapted to KEK requirements L- & S-Band, 50 & 80 MW", Presented on 2017-10-06 in KEK, 2017.

[60] A. Ushakov, talk at a Work shop in 2017 in Itako-Japan.

http://home.hiroshima-u.ac.jp/ mkuriki/2017Itako/

[61] N. Terunuma, talk at a domestic meeting at KEK.

http://atf.kek.jp/twiki/pub/ILCpositron/WeeklyMeetingKEK/Target-_Shielding_Concept.pptx

EDMS Nr.: D00000001165115 Rev: B Ver: 3 Status: Released - for publication Dat.: 23. May 2018

[62] K. Yokoya, talk at LCWS2017 at Strasbourg.
https://agenda.linearcollider.org/event/7645/contributions/40017/attachments-/32323/49050/PositronSourceComparison-LCWS2017.pdf

[63] K. Yokoya, talk at AWLC2017 at SLAC,
https://agenda.linearcollider.org/event/7507/contributions/39226/attachments/31820-/47991/WG1status-AWLC2017-Yokoya.pdf

Positron Working Group

Wei Gai	ANL
Masao Kuriki	Hiroshima Univ.
Benno List	DESY
Gudrid Moortgat-Pick	Hamburg Univ./DESY
Toshiyuki Okugi	KEK
Tsunehiko Omori	KEK
Sabine Riemann	DESY
Peter Sievers	CERN
Tohru Takahashi	Hiroshima Univ.
Nobuhiro Terunuma	KEK
Andriy Ushakov	Hamburg Univ./DESY
Akira Yamamoto	KEK
Kaoru Yokoya (chair)	KEK

We acknowledge the kind help for writing this report by Dr. Shigeki Fukuda (KEK), Dr. Pavel Martyshkin (BINP) and Dr. Yu Morikawa (KEK).